Resilience-based Seismic Design Optimization of typical Highway RC Bridges by Response Surface Method and NSGA-II Algorithm

Sicong Hu (eric731hu@gmail.com)
Nanchang University
Baokui Chen
Nanchang University
Guquan Song
Nanchang University
Lianhua Wang
Hunan University

Research Article

Keywords: Seismic design optimization, Resilience, RC bridges, Elastomeric bearings, Response surface method, NSGA-II

Posted Date: April 1st, 2021

DOI: https://doi.org/10.21203/rs.3.rs-373690/v1

Resilience-based seismic design optimization of typical highway RC bridges by response surface method and NSGA-II algorithm

Sicong Hu[1], Baokui Chen[1], Guquan Song[1], Lianhua Wang[2,3]

Abstract

To maximize the seismic performance and minimize the material cost of the typical highway reinforced concrete (RC) bridges, a resilience-based multi-objective optimal seismic design method is proposed in this study. The size of elastomeric bearings and the cross-section arrangement of RC piers are chosen as the design parameters. To improve the accuracy and efficiency, the nonlinear time history analysis (NTHA) based cloud analysis approach is associated with the response surface method (RSM) to obtain the seismic resilience during the seismic optimization process. Moreover, the optimization problem is solved through an improved version of non-dominated sorting genetic algorithm (NSGA-II) algorithm. Following, the proposed method is applied to a typical highway RC bridge, and the optimal design schemes are determined from the Pareto optimal solutions. The results show that the resilience response surface model can be used to accurately predict the seismic resilience of bridges. The proposed method can adjust the damage grades of various components by considering the contribution of various components, entailing the minimization of material cost and the maximization of seismic resilience.

Key words: Seismic design optimization; Resilience; RC bridges; Elastomeric bearings; Response surface method; NSGA-II.

1. Introduction

Highway bridges play a vital role in the sustainable economic growth and social development. In the past two decades, numerous typical highway RC bridges with similar arrangements are constructed in highway system all over the world. Many of them located in high seismic areas

S Hu (✉) · B Chen · G Song · L Wang (✉)

e-mail: eric731hu@ncu.edu.cn; lhwang@hnu.edu.cn

1 School of Civil Engineering and architecture, Nanchang University, Nanchang, China

2 College of Civil Engineering, Hunan University, Changsha, China

3 Key Laboratory for Wind and Bridge Engineering of Hunan Province, Hunan University, Changsha, China

and required to retain sufficient capacity to withstand a disastrous earthquake. Unfortunately, various bridges were found to suffer damage, which results in the considerable aggravated casualties and economic loss (Basoz and Kiremidjian 1998; Wang and Lee 2009). In fact, unreasonable seismic design is an important factor causing the damage of these bridges during earthquakes. As is well known, the current seismic design guidance doesn't provide the selection of structural alternatives and optimization procedures (Verma and Priestley 1990). Therefore, the design scheme has to be initially tried based on the designer's experience. If the seismic response does not meet the performance target, the design scheme need to be repeatedly revised. In this case, the efficiency of the highly iterative trial-and-error design procedure is strongly sensitive to the professional level and experience of the designer (Sung and Su 2010). By contrast, the optimization seismic design provides a method to obtain the elaborate scheme by using the optimization algorithm. It can solve the deficiency of the current seismic design method and is widely recognized as a valuable tool to perform the cost-effective designs (Papavasileiou and Charmpis 2016). In the past, many studies in the seismic engineering have focused on the transition from the conventional seismic design approach to the optimization seismic design method. Moverover, different performance indicators have been defined as the optimization objectives to propose a more comprehensive and reasonable description of seismic performance. In this respect, the conventional performance indicators, i.e., inner force, ductility level/deformation, were often adopted in the early stages (Verma and Priestley 1990; Sung and Su 2010; Li and Li 2018; Fazli and Pakbaz 2018). With the rapid development of the performance-based seismic design, the damage-based indicators, i.e., damage probability and seismic damage risk, were considered in the seismic optimal design (Xie and Zhang 2018; Gholizadeh and Fattahi 2019).

Recently, the seismic resilience has been attracted more and more attention in the seismic performance assessment of bridges (Bruneau et al. 2003; Dong and Frangopol 2016; Pang et al. 2020; Fu et al. 2020). Generally, the resilience describes the capability of a system to withstand the effects of extreme events and to recover the pre-event performance and functionality promptly and efficiently (Bruneau et al. 2003). It is a comprehensive performance-based assessment content and becoming a driving concept for the new generation of structural design codes (Dong and Frangopol 2016). Bocchini et al. (2014) proposed a resilience-based framework to determine the seismic optimal retrofit prioritization of damage bridges distributed along a highway connection between two cities. Dong et al. (2015) utilized the genetic optimization algorithm to obtain the optimal retrofit action for each bridge within an existing bridge network. Liu et al. (2020) proposed a bi-objective optimization model to

search for non-dominated optimal restoration schedules based on the recovery trajectory. Overall, the previous studies focus on the optimal restoration sequence of bridges in the transportation networks. Whereas, there has been limited study pay attention to the resilience-based optimal design of an individual bridge.

On the other hand, the determination of seismic response is a critical issue in the seismic design optimization. Theoretically, NTHA is the most reliable tool to evaluate the seismic response of structures. However, it was proved to be time-consuming and impractical in the seismic optimization (Rojas et al. 2011). Therefore, the nonlinear static analysis is adopted to improve the efficiency of optimization in many past studies (Verma and Priestley 1990; Sung and Su 2010; Papavasileiou and Charmpis 2016; Li and Li 2018; Fazli and Pakbaz 2018). However, only first mode-dominated multi degree of freedom system can be considered in the nonlinear static analysis. Recently, Mokarram and Banan (Mokarram and Banan 2018) utilized the pushover analysis to preliminary screen the feasible solutions and then used the NTHA to determine the accurate seismic response. Although the approach can accurately obtain the seismic response of structures, the pushover analysis still has an important influence on the selection of the optimal solution. Obviously, the further development of seismic optimization design highly depends on the availability of technology to deal with expensive optimization problems.

Addressing the existing drawbacks and catering to present needs, the main contribution of this work is comprehensively presenting a complete and efficiency framework of the resilience-based seismic design optimization for the typical highway RC bridges. The resilience response surface model is proposed to predict the seismic resilience of bridges during the optimization process, and the NTHA based cloud analysis approach is applied to develop the resilience response surface model. Moreover, this paper is organized as follows. Sect. 2 describes the seismic resilience method of bridges. In Sect. 3, we present the design parameters, objective functions and constraint conditions. The seismic optimal design procedure of RC bridge is proposed in Sect. 4. Subsequently, the details of the case study bridge are described in Sect. 5. Furthermore, the finite element model is developed and the ground motions are selected. Sect. 6 presents the seismic fragility analysis and seismic resilience analysis of the case study bridge. Then, the design optimization results are presented and discussed in Sect. 7. Sect. 8 concludes the paper with some final remarks.

2. Seismic resilience method

Overall, the seismic resilience can be calculated from the normalized area under the functionality curve, as shown in Fig. 1. The occurrence of a seismic event at time t_0 may cause a sudden loss of the bridge functionality. After experienced a delay time δ_d, the functionality of the damaged bridge can be recovered through the post-event restoration activities in the recovery time δ_r. In this case, the seismic resilience is associated with four attributes: robustness, rapidity, redundancy and resourcefulness (Anwar 2020). Considering all attributes together, the seismic resilience of an individual bridge can be defined as:

$$RS|IM = \frac{1}{t_h - t_0}\int_{t_0}^{t_h}[Q(t)|IM]dt, \tag{1}$$

where IM is the specific intensity measure of ground motions; t_h represents the investigated time; $Q(t)$ represents the functionality of a individual bridge under a specify recovery path at time t, which can be obtained by cumulating the residual functionality under different damage states:

$$Q(t)|IM = \sum_{i=0}^{4} Q_{DS_i}(t)|IM, \tag{2}$$

where DS_i is the damage state (i.e., DS_0 denotes no damage, DS_1 denotes the slight damage, DS_2 denotes the moderate damage, DS_3 denotes the extensive damage and DS_4 denotes the complete damage **Error! Reference source not found.**).

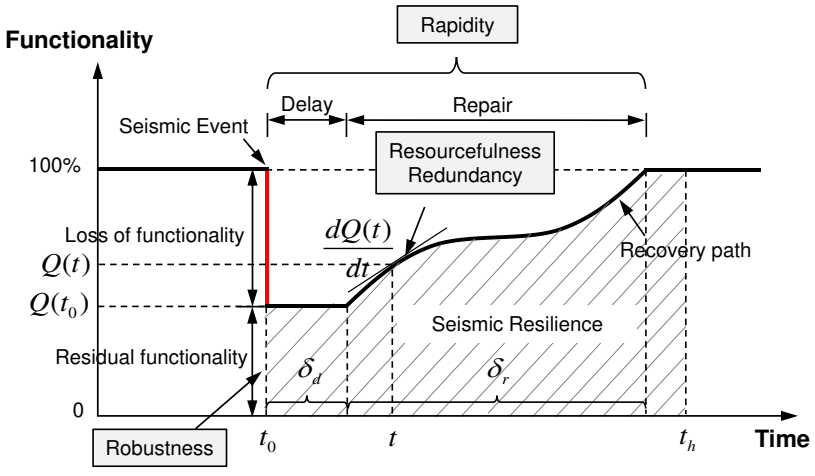

Fig. 1 Schematic representation of seismic resilience

Bridge functionality under different damage states can be quantified by mapping the current damage state to a functionality value between 0 and 1. Specifically, the bridge functionality under different damage states at t_0 can be written as:

$$Q_{DS_i}(t_0)\,|IM = 1 - (P_{DS_i}|IM - P_{DS_{i+1}}|IM) \times C_{DS_i}, \tag{3}$$

where $P_{DS_i}|IM$ and $P_{DS_{i+1}}|IM$ are the exceedance probability of a bridge at different damage states; C_{DS_i} is the functionality loss ratio associated with different damage states. Subsequently, the functionality of a bridge at the specific time t can be determined as follows:

$$Q_{DS_i}(t)\,|IM = Q_{DS_i}(t_0)\,|IM + H(\tau) \times f(\tau) \times [Q_{DS_i}(t_h)\,|IM - Q_{DS_i}(t_0)\,|IM], \tag{4}$$

where $\tau = (t - t_0 - \delta_d)/\delta_r \in [0, 1]$ is a normalized time variable; $H(\tau)$ is the Heaviside unit step function; $f(\tau) \in [0, 1]$ is the recovery models.

Strictly speaking, the recovery process is related to the resources available after the seismic event and the role of the damaged components in the system performance (Biondini 2015). However, the following models are commonly applied to approximately reflect the recovery process (Dong and Frangopol 2016; Pang et al. 2020; Fu et al. 2020):

$$f(\tau) = \begin{cases} 1 - e^{-k\tau} & \text{slight damage} \\ [1 - \cos(\pi\tau)]/2 & \text{moderate damage} \\ e^{-k(1-\tau)} & \text{extensive/ complete damage} \end{cases}, \tag{5}$$

where k is a shape parameter.

On the other hand, the exceedance probability of a bridge at each damage state $P_{DS_i}|IM$ can be described by the seismic fragility functions. Overall, the seismic fragility function is defined as the conditional probability of the seismic demand exceeding the seismic demand. If we assume that the seismic demand and seismic capacity follow lognormal distributions, the seismic fragility function can be expressed as (Nielson and DesRoches 2007):

$$P_{DS_i}|IM = P[S_D > S_{C,DS_i}|IM] = \Phi\left[\left.\frac{\ln\left(\overline{S_D}/\overline{S_{C,DS_i}}\right)}{\sqrt{\beta_D^2 + \beta_{C,DS_i}^2}}\right| IM\right], \tag{6}$$

where S_D is the structural seismic demand for the specific IM; S_{C,DS_i} is the structural seismic capacity corresponding to the given DS_i; $\overline{S_D}$ and $\overline{S_{C,DS_i}}$ represent the median estimate of the seismic demand and seismic capacity, respectively; β_D and β_{C,DS_i} represent the standard deviation of the seismic demand and seismic capacity, respectively; $\Phi[\cdot]$ is the standard normal cumulative distribution function.

Theoretically, $\overline{S_{C,DS_i}}$ and β_{C,DS_i} can be obtained by the probability seismic capacity model (PSCM). The probability seismic demand model (PSDM) can be develop to determine the relationship between $\overline{S_D}$ and IM as follows:

$$\overline{S_D} = a \ln(IM) + b, \tag{7}$$

where a and b are the regression coefficients. Moreover, the standard deviation of seismic demand β_D can be determined as follows:

$$\beta_D = \sqrt{\frac{\sum_{m=1}^{N}[\ln(S_{D,m}) - \ln(aIM_m^b)]}{N-2}}, \tag{8}$$

where $S_{D,m}$ is the actual seismic demand for a given IM; N is the number of simulations. According to the method, the NTHA based cloud analysis approach is applied to obtain the seismic fragility functions of bridge components. In this approach, a series of nonlinear time history analysis is performed using a set of unscaled ground motion records. A set of IM values and their associated seismic demand values of each component can be obtained and the PSDM can be determined by the regression analysis. Based on the PSDMs, the fragility functions of bridge components can be developed. Furthermore, the joint probabilistic seismic demand models (JPSDMs) are developed using the vector of seismic response mean of each component and the correlation coefficient matrix of seismic response of different components (Nielson and DesRoches 2007; Choi et al. 2004). Using the seismic capacities and JPSDMs, the Monte Carlo simulation is adopted to obtain random samples of the seismic capacity and seismic demand of bridge systems at different IMs for each damage state. The number of damage samples is counted and a regression analysis is applied to estimate the seismic fragility functions of bridge systems.

3. Seismic optimization model

3.1 Optimization parameters

The type of highway RC bridges that shown in fig 2 is widely used in the transportation network owing to its simple structure and easy construction. Overall, the pier is designed to have double circular columns and a bent. Moreover, the elastomeric bearings and the PTFE elastomeric bearings are respectively arranged at the top of the bents and abutments to balance the internal force and deformation. Obviously, the cross-section arrangement of the piers and the sizes of the elastomeric bearings play an important role in the seismic performance of bridge. In this respect, the following five parameters can be chosen as the optimization parameters: the total thickness of rubber layers in elastomeric bearings T_e, the rubber area of elastomeric bearings A_e, the diameter of piers D, the longitudinal reinforcement ratio of piers ρ_s and the volumetric ratio of transverse reinforcement ρ_h.

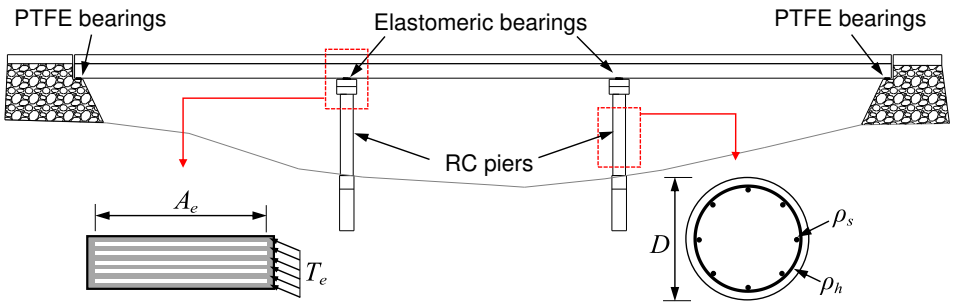

Fig. 2 Optimization parameters of the typical RC bridge

3.2 Objective functions

In general, the primary objective of seismic optimization is to minimize the material cost and maximize the seismic performance. In this study, the seismic resilience of bridge system is adopted to quantify the seismic performance of bridges, and the total material cost of the RC piers and elastomeric bearings are used to roughly describe the material cost of bridges. In this case, the objective functions can be expressed as:

$$\begin{cases} \text{Maxmize} & RS|IM_D\,(T_e, A_e, D, \rho_s, \rho_h) \\ \text{Minimize} & C(T_e, A_e, D, \rho_s, \rho_h) \end{cases}, \tag{9}$$

where $RS|IM_D$ is the seismic resilience of bridge systems under a design intensity level (IM_D) earthquake; C is the total material cost of the RC piers and elastomeric bearings, which can be determined as:

$$C = C_{Bearing} + C_{Pier} = C_{Bearing} + (c_c + c_h \rho_h + c_s \rho_s) V_c\,, \tag{10}$$

where $C_{Bearing}$ and C_{Pier} are the material cost of the elastomeric bearings and RC piers, respectively; V_c is the volume of concrete in a pier; c_c, c_h, c_s are the material cost per volume of concrete, longitudinal reinforcement and transverse reinforcement, respectively.

3.3 Constraint conditions

In order to ensure the optimization parameters satisfy the project requirements and design standards, the following constraint conditions should be considered during the optimization process.

(1) Piers

The shear capacity of the RC piers V should satisfy the following conditions to avoid the brittle failure (MOHURD 2011):

$$V = 0.85\,(V_c + V_s)/1.2 \geq V_y\,, \tag{11}$$

where V_y is the seismic shear demand of the RC piers; V_c and V_s are the concrete and reinforcement contribution to the shear capacity, respectively. They can be determined as follows:

$$V_c = 0.085A_g \times \min\left[\lambda\left(1+\frac{P}{1.38A_g}\right)\sqrt{f_c}, 0.335\sqrt{f_c}, 1.47\lambda\sqrt{f_c}\right], \tag{12}$$

$$V_s = \min\left(0.05\sqrt{f_c}\,A_g\rho_h f_{yh}, 0.064\sqrt{f_c}\,A_g\right), \tag{13}$$

where A_g is the gross area of cross section; λ is the coefficient related to the displacement ductility ratio; P is the lowest axial force of piers; f_c is the concrete compressive strength; f_{yh} is the yield strength of transverse reinforcement.

Moreover, the longitudinal reinforcement ratio and the volumetric ratio of transverse reinforcement of RC piers should satisfy the following conditions:

$$\begin{cases}\rho_{h,\min} \leqslant \rho \leqslant \rho_{h,\max} \\ \rho_{s,\min} \leqslant \rho \leqslant \rho_{s,\max}\end{cases}, \tag{14}$$

where $\rho_{h,\,\min}$ and $\rho_{s,\,\min}$ are the minimum requirement of reinforcements; $\rho_{h,\,\max}$ and $\rho_{s,\,\max}$ are the maximum allowable values of reinforcements.

(2) Elastomeric bearings

In order to provide appropriate load and movement capacities at the service limit state, the area of the elastomeric bearings and the total thickness of the rubber layers should satisfy the following conditions (HPDIMC 2018):

$$\begin{cases}A_e \geqslant \dfrac{R_b}{\sigma_r} \\ T_e \geqslant 2\Delta t\end{cases}, \tag{15}$$

where R_b is the maximum vertical reaction force of the elastomeric bearing at the service limit state; σ_r and Δt are the allowable compression stress and shear deformation of the elastomeric bearings, respectively.

Generally, the above constraint conditions are handled by using the penalty functions method in this study. Therefore, the penalized objective function F_p can be defined as follows:

$$F_p = F + \sum_{k=1}^{n}\alpha_k\delta_k, \tag{16}$$

where F is the unpenalized objective function, see Eq. (9); α_k is the penalty parameter imposed for violation of constraint functions; $\delta_k = \begin{cases}g_k & if \quad g_k > 0 \\ 0 & if \quad g_k \leqslant 0\end{cases}$ is a violation factor for the k constraint functions; g_k is the constraint function.

4. Seismic optimal design method

4.1 Response surface method

Theoretically, the objective function values of samples should be iteratively calculated during the optimization process. Therefore, determining the objective function quickly is critical to improving the efficiency of optimization. As mentioned, the material cost can be simplify calculated via Eq. (10). Whereas, the seismic resilience analysis includes large scale nonlinear time history analysis, which will result in an inefficient multi-objective optimization process. To solve this problem, the RSM is applied to establish the relationship between the seismic resilience of bridge systems and optimization parameters in this study. In this case, the seismic resilience can be obtained from the resilience response surface model instead of the full process seismic resilience analysis.

As a statistical method, the RSM can establish a prediction model via the multivariate nonlinear regression. According to this method, the seismic resilience can be described as follows:

$$RS = \widehat{RS} + \varepsilon = \mathbf{aX} + \varepsilon, \tag{17}$$

where $\widehat{RS}$ is the approximate seismic resilience; $\mathbf{a}$ represents the vector of the regression coefficients; $\mathbf{X} = [X_1, X_2, \cdots, X_n]$ represents the vector of the design parameters; ε is the residual error.

For the practical engineering applications, a second-order polynomial function with the cross terms is adequate and appropriate to represent their structural performance functions. Therefore, the estimated resilience response surface model can be expressed by Eq. (18).

$$\widehat{RS} = a_0 + \sum_{i=1}^{n} a_i X_i + \sum_{i=1}^{n} a_{ii} X_i^2 + \sum_{i=1}^{n} \sum_{j=i+1}^{n} a_{ij} X_i X_j, \tag{18}$$

where a_i and a_{ij} are the regression coefficients.

It should be pointed out that the coefficients of response surface model should be determined by performing a set of experiment runs. Therefore, it is important to select appropriate sample points to represent the characteristics of the actual function in the whole design space. In this respect, the central composite design (CCD) is a type of design of experiments techniques, which provides the needed basis for selecting sample points (Box and Wilson 1951). For the two-level three-factorial design, the CCD consists of 20 experimental runs with 6 at central point, 6 at axial point and 8 at factorial point, as shown in Fig. 3. For these points, factor values are usually rescaled (coded): factorial points= ±1, centre points= 0, and axial points= $\pm a$ (one factor) and 0 (the other factor).

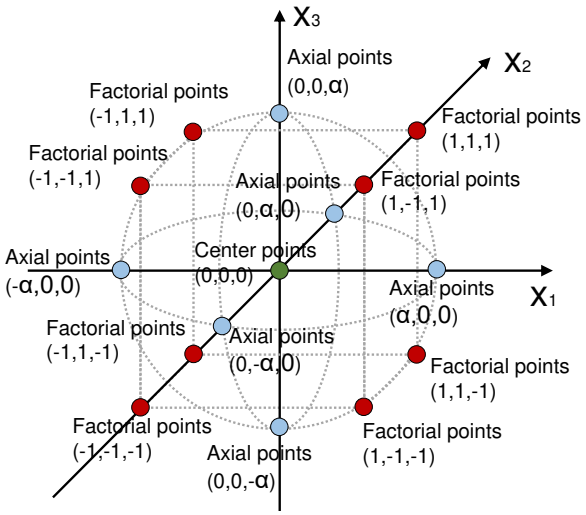

Fig. 3 Design points of central composite design method

Based on the seismic resilience of each sample point, the regression coefficients in Eq. (18) can be estimated by the least squares estimators. Then, an estimated response surface model should be validated to check its accuracy and reliability for the further applications. Generally, the determination coefficient R^2, adjusted determination coefficient R^2_{adj} and the root mean square of errors RMSE are used herein for the validation.

4.2 NSGA-II algorithm

Overall, five optimization parameters and two objective functions are included in the proposed optimization model. Therefore, it is a multi-objective optimization process. Unlike the single-objective optimization can determinate the single solution, the multi-objective optimization usually obtains an optimal solution set, which is called the Pareto optimal solutions. In this study, the multi-objective optimization is executed by the NSGA-II algorithm (Deb et al. 2002).

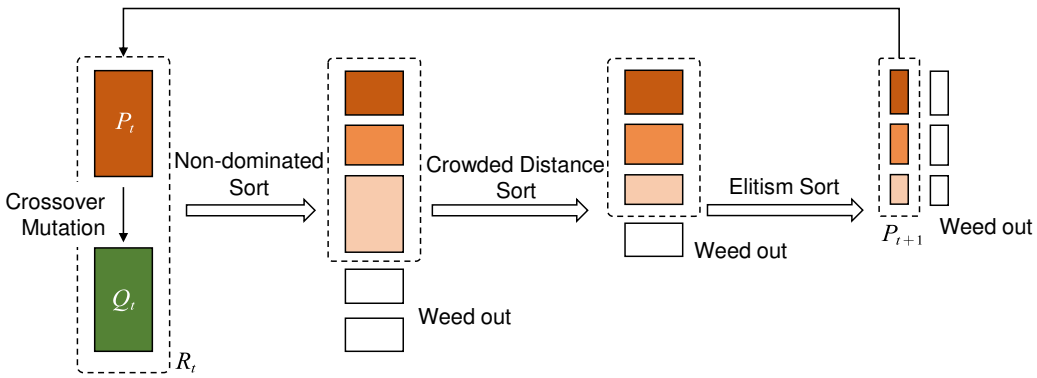

Fig. 4 Flowchart of the NSGA-II method

Fig.4 shows the principle of NSGA-II algorithm. Generally, the initial population is randomly generated and is sorted based on the non-domination level and the crowded distance metric. Then, the first generation population is obtained through the genetic operations, i.e., selection, crossover and mutation. From the second generation, the parent population and the child population are simultaneously merged to perform the fast non-dominated sorting, crowded distance sort and elitism sort. Subsequently, individuals with better fitness are selected to generate new parent population. Finally, the genetic operations are repeatedly applied to produce new offspring populations until the end of the simulation yields the Pareto solutions.

4.3 Seismic optimal design process

Based on the resilience response surface model and the NSGA-II algorithm, the resilience-based seismic optimization design process of bridges are summarized in Fig. 5. Overall, four main parts are included in the process:

Part 1: Develop resilience response surface model. According to the engineering practices, the meaningful ranges of design parameters are firstly determined. Then, the bridge samples including various design parameters are generated via the CCD method, and the seismic resilience analysis is performed (Part. 2). Finally, the resilience response surface model is developed by fitting the seismic resilience data points of all bridge samples (Eq. (18)).

Part 2: Perform seismic resilience analysis. The seismic demand and seismic capacity of bridge components are determined by the nonlinear time history analysis and nonlinear static analysis, respectively. Then, the seismic fragility functions are developed by comparing the seismic demand and seismic capacity (Eqs. (6)~(8)). Following, the damage probabilities of bridges suffering the design level earthquake are obtained and the residual functionalities of damage bridges are determined via Eqs. (2) and (3). Moreover, the functionality recovery process of damage bridges can be determined via Eqs. (4) and (5). Finally, the seismic resilience of bridge can be obtained by Eq. (1).

Part 3: Obtain Pareto optimal solutions. The parameters of NSGA-II algorithm are firstly determined. Then, the bridge samples are randomly generated and are regarded as the initial population. The material cost of bridge samples are calculated by Eq. (10) and the seismic resilience of bridge samples are determined by the resilience response surface model. Moreover, the constraint conditions are judged and the penalized objective functions are calculated by Eq. (16). Finally, the NSGA-II algorithm is performed to obtain the Pareto optimal solutions.

Part 4: Determine optimal design scheme. The optimal design scheme can be finally determined from the Pareto optimal solutions by considering the specific optimization strategies. Overall, three individuate optimal strategies are proposed in this study: Strategy 1 maximizes the seismic resilience of bridge without increasing the material cost; Strategy 2 maintains the seismic resilience of bridge and minimizes the material cost; Strategy 3 controls the benefit cost ratio (BCR) no less than a specific proportion of the maximum BCR in the Pareto optimal solution set.

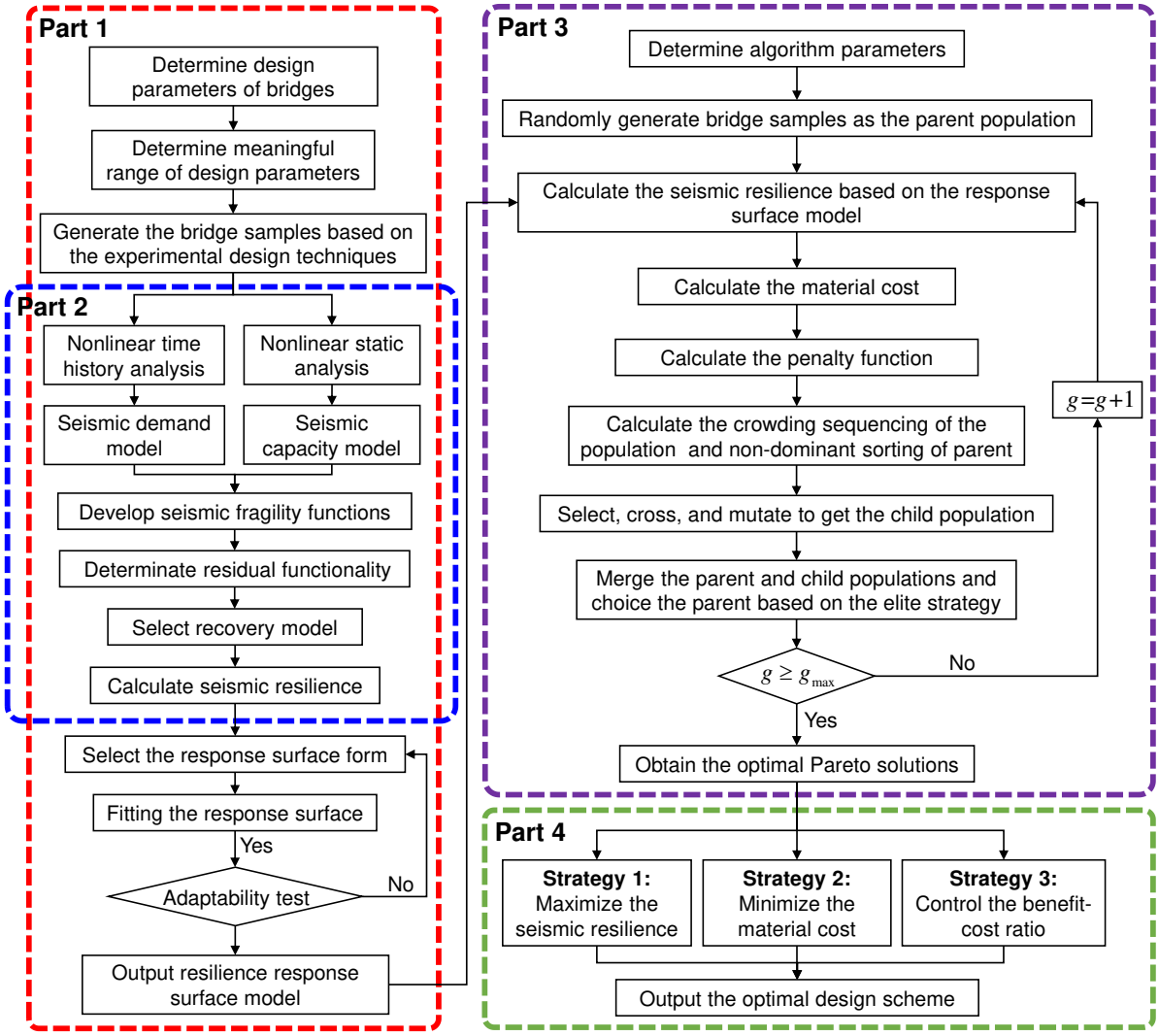

Fig. 5 Flow chart of the resilience-based seismic optimization design process of RC bridges using RSM and NSGA-II

5. Case study bridge

In this study, a continuous RC bridge with spans of 3×30m is selected as the case study, as shown in Fig. 6. The width and height of the deck are 13.25m and 1.6m, respectively. The substructure is made up of two abutments and four piers. The height and diameter of piers are

10m and 1.4m, respectively. The concrete strengths of the substructure and superstructure are 30MPa and 50MPa, respectively. The piers are reinforced by the HRB335 longitudinal reinforcement and spiral hoop. Both of the longitudinal reinforcement ratio and the volumetric ratio of transverse reinforcement are 1.5%. Meanwhile, eight elastomeric bearings are installed at the top of each bent, and eight PTFE elastomeric bearings are located on the top of each abutment. The total thickness of the rubber layers in the elastomeric bearings is 0.1m and the area of the elastomeric bearings is 0.1m^2. The shear strength of the elastomeric bearings is 10MPa. Moreover, the concrete shear keys are set up at the transverse direction of the bridge.

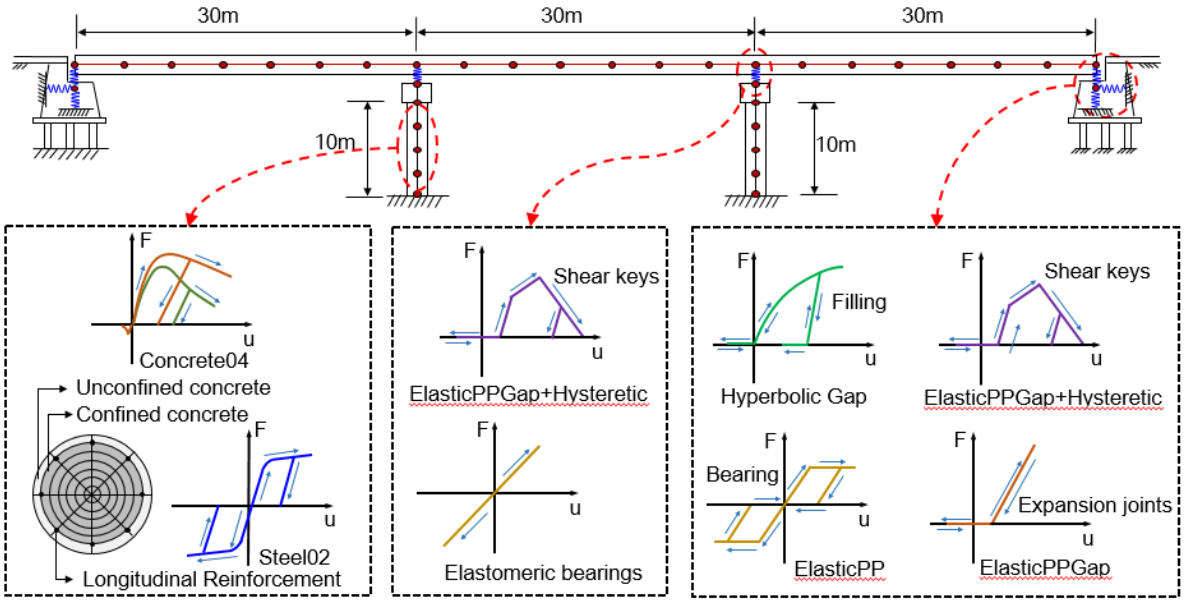

Fig. 6 Schematic and finite element model of the case study bridge

The nonlinear finite element model of the case study bridge is developed by using OpenSees (McKenna 2000), as shown in Fig. 6. Overall, the elastic beam-column element is used to simulate the superstructure, whereas the distributed plasticity fiber-element model is used to simulate the piers. For the fiber-element model of columns, the stress-strain relationship of the confined and unconfined concrete is modeled as the Concrete04 material, while that of the longitudinal reinforcement is simulated as the Steel02 material. The zero length elements with the Elastic and ElasticPP materials are applied to simulate the elastomeric bearings and the PTFE bearings, respectively. The shear keys are simulated in parallel with the Hysteretic and ElasticPPGap materials. The pounding effects between the deck and abutments are accounted for using the ElasticPPGap material. The interaction effects of the abutments and backfill soil are simulated by using HyperbolicGap material (Wilson and Elgamal 2010). The static analysis presents the maximum vertical reaction force and maximum shear deformation of a single

elastomeric bearing at the service limit state are 850kN and 0.06m, respectively. Moreover, the modal analysis presents the first two periods of the bridge are 2.52s and 1.98s, respectively. On the other hand, 100 ground motions are selected from the PEER strong motion database to perform the seismic fragility and resilience analysis (Shome et al. 1998). The selected ground motions include different source-to-site distances and magnitudes (Fig. 7(a)): small magnitude and small epicentre distances (SMSR), small magnitude and large epicentre distances (SMLR), large magnitude and small epicentre distances (LMSR), large magnitude and large epicentre distances (LMLR), near field (NF). Moreover, the PGV is considered as the intensity measures to reduce the dispersion in predicting seismic demand. Fig. 7(b) shows the corresponding PGV distribution of the selected ground motions.

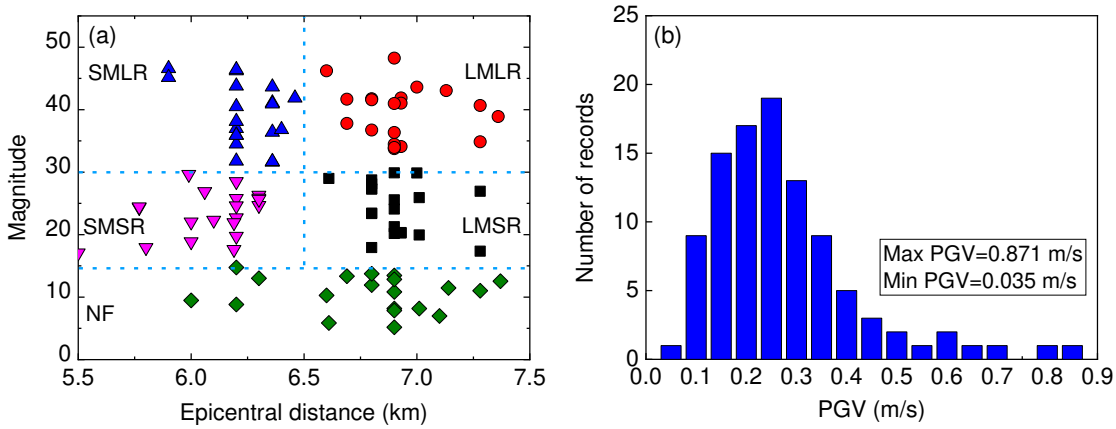

Fig. 7 (a) Distribution of ground motion records in M-R space and (b) histogram of the PGV for ground motion records

6. Fragility and resilience analysis

In this study, six kinds of critical bridge components, i.e., piers, shear keys at abutment, shear keys at bent, PTFE bearings, elastomeric bearings and abutments, are considered during the seismic fragility and resilience analysis. The seismic capacity of each component at different damage states are listed in Table 1 (Hu et al. 2019).

Table 1 Seismic capacity of components at various damage states

Components	Damage Index	Slight	Moderate	Extensive	Complete
Piers	Curvature ductility	1	1.62	5.43	12.48
Shear keys at Abutment	Deformation (mm)	5.2	51	70	130
Shear keys at bent	Deformation (mm)	5.2	51	70	130
PTFE bearings	Displacement (mm)	80	150	200	300
Elastomeric bearings	Shear strain	100%	150%	200%	250%
Abutment	Deformation (mm)	5.5	11	35	100

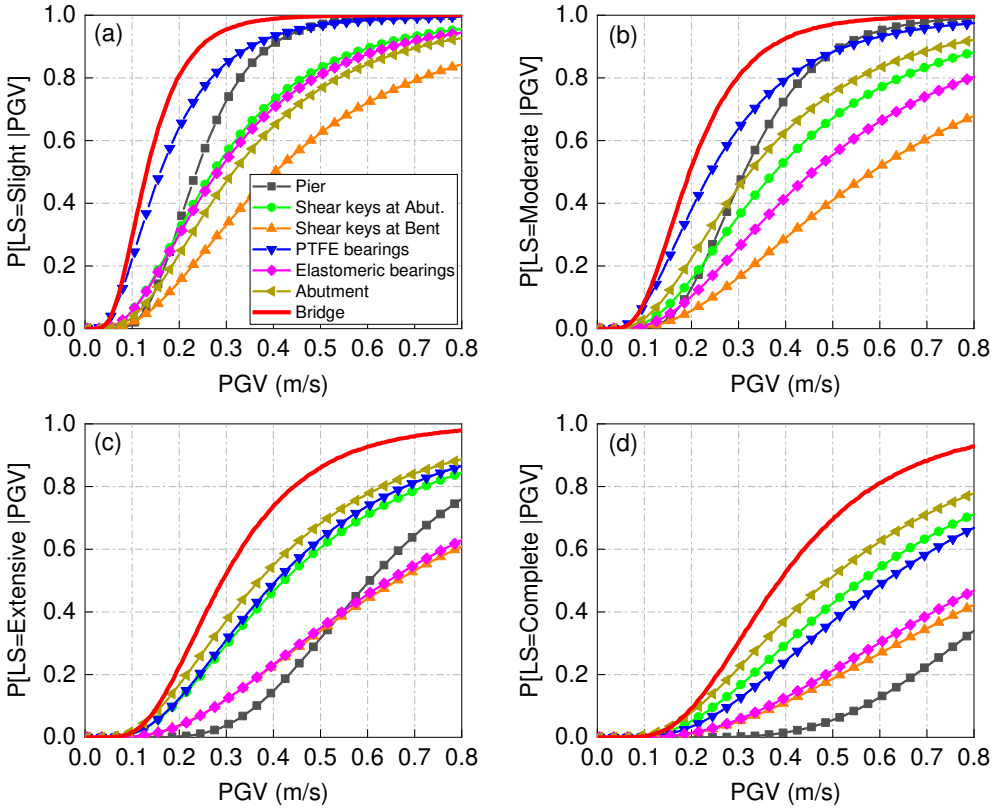

Fig. 8 Fragility curves of components and bridge at four damage states: (a) slight damage, (b) moderate damage, (c) extensive damage and (d) complete damage

Fig. 8 shows the fragility curves of different bridge components and bridge system at four damage states. It should be noted that each kind of the components has several subcomponents and the most vulnerable subcomponent is selected and present in the figure. The stiffness of abutments is larger than that of piers, entailing the deformation demand of PTFE bearings is significantly larger than that of elastomeric bearings. Therefore, it can be observed that the PTFE bearings are more vulnerable than the elastomeric bearings at four damage states. Similarly, the damage probabilities of shear keys at abutments are higher than those at piers. The piers appear to be the second fragile component at the slight and moderate damage states. Whereas, the exceedance probabilities at extensive and complete damage states of piers are very small. Therefore, the piers is expected to exhibit excellent ductility. Moreover, the gaps of expansion joints make the exceedance probabilities of abutment at slight damage state slighter than those of most components. However, the abutment becomes the most fragile component at high level damage states (i.e., extensive and complete damage) because of its low ductility. On the other hand, the bridge system fragility curves indicated that the bridge system is more fragile than any one of the bridge components. Obviously, it is more appropriate to adopt system-level performance indicator than component-level performance indicator

while seismic design. Overall, the damage probabilities of the bridge system considered in here are considered governed by the PTFE bearings and piers at the slight and moderate damage states. Moreover, the abutments, shear keys at abutment and PTFE bearings paly an important role in the extensive and complete damage of the bridge system.

According to the seismic fragility curves, the residual functionality and functionality recovery processes of the bridge can be further determined. Table 2 summarizes the probability distributions of the random variables in the seismic resilience analysis. Fig. 9 (a) presents the distribution of the functionality after bridge suffering a ground motion with PGV=0.4 m/s. It can be observed that the bridge functionality reduces rapidly at first and then increases slowly. Generally, the high level damage has more significant contributes to the degradation of bridge functionality than the low level damage (i.e., slight and moderate damage). At the same time, the high level damage need a longer recovery time than the low level damage. Therefore, the functionality recovery ratio in the early stage is relatively lower than that in the later stage. Moreover, the recovery process in the later stage presents a significant dispersion. Fig. 9 (b) presents the functionality recovery processes of the bridge under different intensity of ground motions. As expected, the residual functionality will reduce with the PGV increases. Moreover, the proportion of high level damage will increase with the PGV increases, entailing the nonlinear characteristics of recovery processes more significant. In this case, the recovery of functionality is mainly concentrated in the later stage.

Table 2 Probability distributions of random variables in the seismic resilience analysis

Parameter	Unit	Distribution Type	Upper	Lower	Mean	References
δ_d	days	Uniform distribution	60	30	45	Pang et al. (2020)
δ_{r,DS_1}	days	Triangular distribution	1	0.2	0.6	Dong and Frangopol (2016)
δ_{r,DS_2}	days	Triangular distribution	5	1	2.5	Dong and Frangopol (2016)
δ_{r,DS_3}	days	Triangular distribution	120	30	75	Dong and Frangopol (2016)
δ_{r,DS_4}	days	Triangular distribution	360	120	230	Dong and Frangopol (2016)
C_{DS_1}	-	Determined value	-	-	0.03	Fu et al. (2020)
C_{DS_2}	-	Determined value	-	-	0.08	Fu et al. (2020)
C_{DS_3}	-	Determined value	-	-	0.25	Fu et al. (2020)
C_{DS_4}	-	Determined value	-	-	0.67	Fu et al. (2020)
k	-	Uniform distribution	10	8	0.8	Pang et al. (2020)

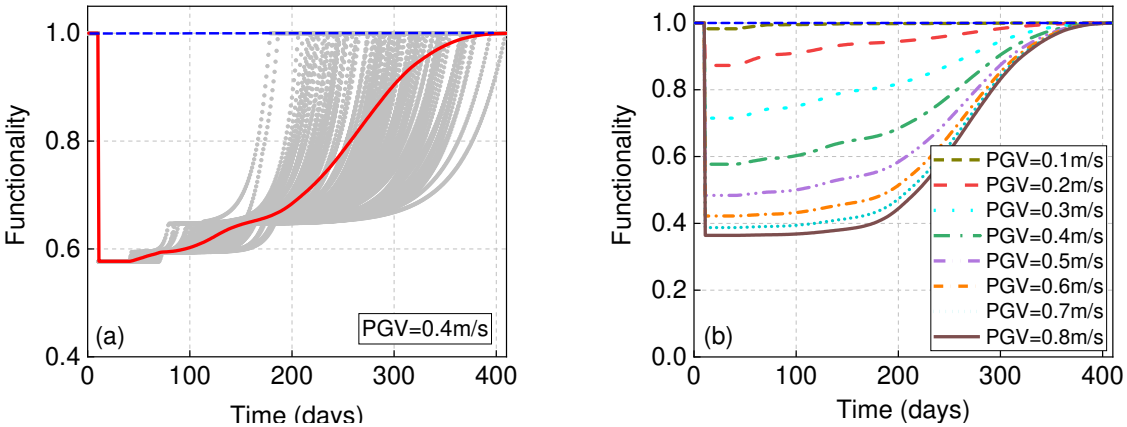

Fig. 9 (a) Random samples of functionality recovery processes at PGV=0.4 m/s and (b) average functionality recovery processes with varied PGVs

Following, the seismic resilience of the bridge can be finally determined by assuming the control times is 400 days. Fig. 10 shows the mean values and ranges of the seismic resilience with varied PGVs. Because of the various proportion of four damage states, the seismic resilience of bridge presents a nonlinear variation with the PGV increase. In particular, the bridge mainly incurs low level damage when the PGV is less than 0.1m/s. As a result, the decrease rate of the seismic resilience is small in this range. Whereas, the seismic resilience decreases quickly as the PGV increases. Moreover, the uncertainty of the seismic resilience presents a significantly increase with the rise of the PGV.

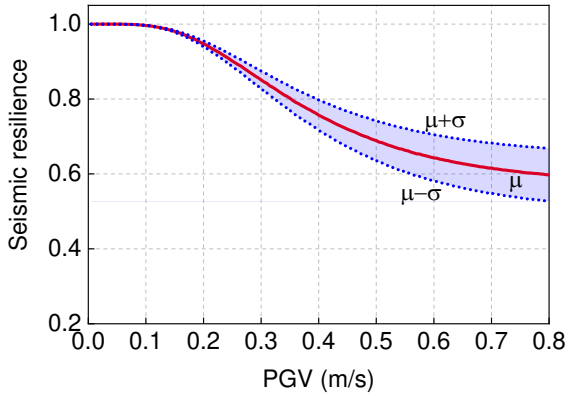

Fig. 10 Seismic resilience of bridge with varied PGVs.

7. Seismic design optimization

7.1 Resilience response surface

As stated, the resilience response surface model should be developed before the seismic optimization design. Based on the engineering judgments, the ranges of the design parameters

411 are determined and the factor level are listed in Table 3. According to the CCD, 50 bridge
412 samples are generated. Moreover, α is chosen as 2.37841 to satisfy the rotatability properties.
413 Similar to the process in Sec. 6, the seismic resilience of each bridge sample is determined. In
414 this study, the design seismic intensity is assumed as 0.4m/s. Based on the average seismic
415 resilience at PGV=0.4 m/s, the statistical significance of each factor term is determined by the
416 analysis of variance (ANOVA) with quadratic models. Fig. 11 shows the *p*-value of each factor
417 term in the response surface model. It is seen from the figure that T_e, A_e, D, D^2, ρ_h, $T_e D$
418 are extremely significant levels terms ($p \leqslant 0.001$), while $A_e D$ and $D\rho_s$ are very significant
419 levels terms ($p \leqslant 0.01$). Moreover, $T_e \rho_s$ and T_e^2 are significant levels terms ($p \leqslant 0.05$).
420 Whereas, other factor terms are not significant.

421 Table 3 Factor level of the design parameters

Level	t_e (m)	A_e (m^2)	D (m)	ρ_s (%)	ρ_h (%)
-2.378	0.030	0.10	1.00	0.70	0.30
-1	0.056	0.13	1.29	1.66	1.08
0	0.075	0.15	1.50	2.35	1.65
1	0.094	0.17	1.71	3.04	2.22
2.378	0.120	0.20	2.00	4.00	3.00

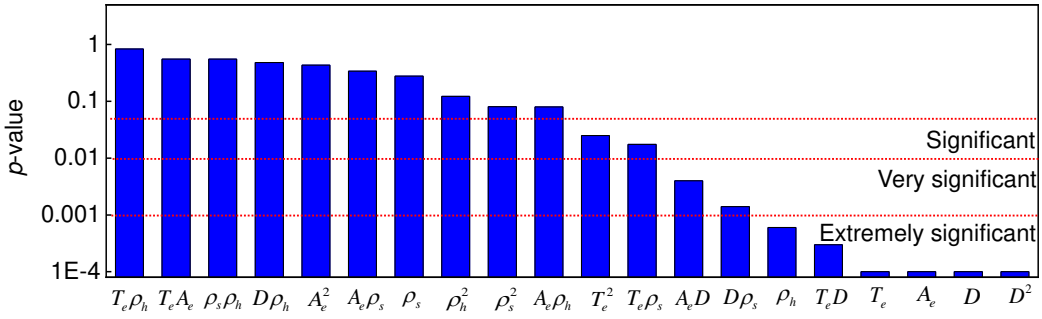

422
423 Fig. 11 Pareto effect diagram for each factor term.

424 After rounding off the insignificant items, the simplified resilience response surface model can
425 be described as follows:

$$\begin{aligned} RS = {} & 0.4 - 0.3T_e - 0.25A_e + 0.5D - 7.76\times10^{-4}\rho_s + 0.012\rho_h \\ & -0.85T_eD + 0.159T_e\rho_s + 0.49A_eD - 0.105A_e\rho_h \\ & -0.016D\rho_s + 4.05T_e^2 - 0.138D^2 + 2.24\times10^{-3}\rho_s^2 \end{aligned} \tag{19}$$

426

427 Table 4 Determination coefficient of the resilience response surface model

Response factor	R^2	R_{adj}^2	RMSE
RS	0.964	0.955	0.00394

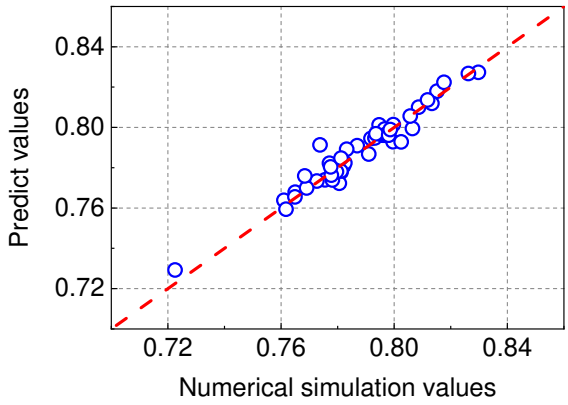

Fig. 12 Response variables obtained from the numerical simulations and resilience response surface model.

Table 4 lists the determination coefficients of the resilience response surface. It can be seen that the R^2 and R_{adj}^2 are greater than 90%, and the RMSE is very small. Moreover, Fig. 12 shows the seismic resilience obtained from the numerical simulations and resilience response surface model. It is seen that the values ranges from 0.733 to 0.834. A good correlation can be observed from the figure. Obviously, the accuracy of the resilience response surface model can satisfies the following analysis (Papila and Haftka 2000).

7.2 Pareto solutions

To calculate the material cost, we assume that the unit costs of concrete and reinforcement steel are \$105/m^3 and \$7065/m^3, respectively. Moreover, the cost of the elastomeric bearings can be crudely determined as follows (Fazli and Pakbaz 2018):

$$C_{Bearing} = 9623A_e + 7764t_e + 12\,, \tag{20}$$

After obtaining all objective functions, the NSGA-II algorithm is performed to find optimized solutions. A population size of 5000 is used in the algorithm runs. Moreover, the crossover and mutation probabilities are 0.8 and 0.1, respectively. Figure 13 (a) shows the Pareto optimal solution set under different runs. It can be seen that the initial population is widely distributed in the solution space and the Pareto optimal solutions trend to convergence after 40 runs. Moreover, the Pareto optimal solution set is continuous and has a wide coverage and uniform distribution. Obviously, the population sizes and evolution times are enough for the seismic optimization design. Moreover, the Pareto optimal solution set clearly reflects the conflict relationship between the seismic resilience and material cost, which means that the increases of the seismic resilience will result in an increase of the material cost. Moreover, the nonlinear relationship between the material cost and the seismic resilience of bridge can be observed.

When the seismic resilience is low, the slope of Pareto frontier is small. In this range, the seismic resilience can be easily improved by increasing the material costs. Whereas, the slope of the Pareto frontier increases as the seismic resilience increases. Therefore, we can reasonably conduct that the increase of the material costs does not always beneficial to improve the seismic resilience.

According to the Pareto optimal solution set, the optimization schemes of the case bridge can be further determined by considering the specific optimization strategies. As stated in Sec. 4, we consider three optimization strategies in this study. The allowance BCR is set as 50% of the maximum BCR in the Pareto optimal solution set. Figure 13 (b) shows the three optimization schemes. Table 5 summarizes the design parameters and objective functions of bridge before and after the optimization. Referring to Fig. 13 (b), the original scheme is far from the Pareto solution set, which implies the original scheme has great potential for improvement in seismic resilience and economy. In fact, we can observed from Table 5 that the seismic resilience of the optimization scheme 1 increases by 8%. For the optimization scheme 2, the material cost is reduced by nearly 30%. By contrast, the seismic resilience and material cost of the optimization scheme 3 are relatively balance. It can be inferred that the method can reasonably determine the design scheme according to the weight between the material cost and seismic resilience. To verify the correctness of the optimization scheme, the bridges with three optimal schemes are re-submitted to the seismic resilience analysis. The numerical simulation (NS) of seismic resilience is also listed in Table 5. The relative error of each seismic resilience value is within 0.4% in the three optimization schemes. As a result, the optimized scheme obtained by combining response surface method and numerical simulation is highly reliable.

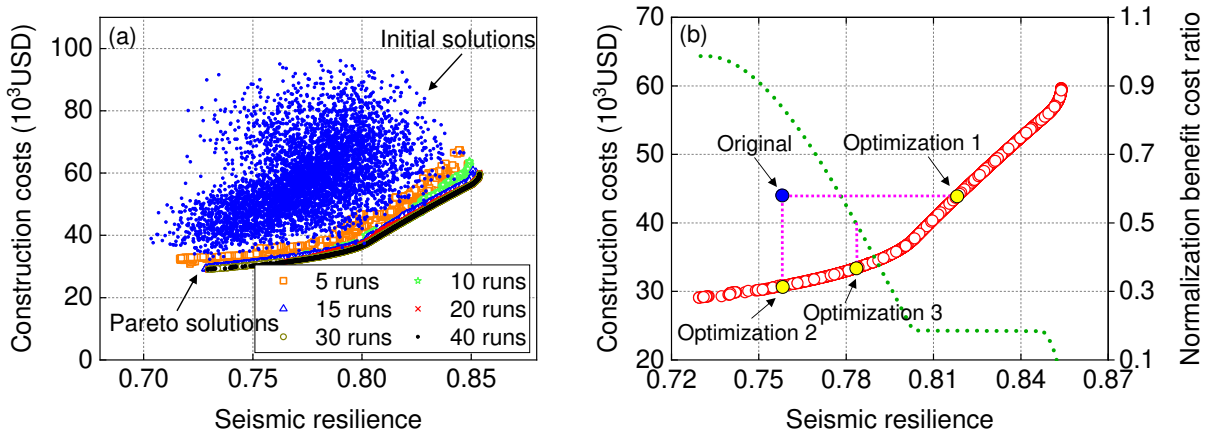

Fig. 13 (a) Initial solutions and Pareto solutions with different runs and (b) optimization schemes.

As stated, the PTFE bearings, abutments and shear keys at abutments are vulnerable components in the bridge system. In this case, the decrease in the total thickness of rubber layer and the increase in the area of elastomeric bearings are benefit to reducing the displacement of girder, entailing the decrease of seismic damage of the above components. However, the latter will result in the rise of material cost at the same time. Therefore, it can be seen from Table 5 that the total thickness of elastomeric bearings decrease to the lower bound in the three optimization schemes, whereas the increase in the area of elastomeric bearings only exists in the optimization scheme 1. On the other hand, the transverse reinforcement plays an important role in improving the ductility of RC piers. However, the bridge isn't governed by the RC piers at extensive and complete damage states. Therefore, the minimum volumetric ratio of transverse reinforcements is adopted in the three optimization schemes to save the material cost. Moreover, both the increase in the diameter of cross section and longitudinal reinforcement ratio has positive influence on controlling the slight and moderate damage of RC piers. Due to the relatively low cost of concrete than reinforcement, the longitudinal reinforcement ratio decrease to the lower bound, whereas the diameter of cross section fluctuates with the vary of optimization strategies.

Table 5 Optimization parameters and objective functions with different design schemes

Parameters /objective functions	Unit	Original	Opt. 1	Opt. 2	Opt. 3
T_e	m	0.1	0.06	0.06	0.06
A_e	m^2	0.1	0.14	0.1	0.1
D	m	1.4	1.63	1.15	1.32
ρ_s	%	1.5	0.7	0.7	0.7
ρ_h	%	1.5	0.3	0.3	0.3
Material costs	$	44091	44089	30887	33279
Seismic resilience (RSM)	-	0.7579	0.8187	0.7581	0.7827
Seismic resilience (NS)	-	0.7577	0.8165	0.7567	0.7859

Fig. 14 presents the fragility curves of the original and optimized bridge at moderate and complete damages. At the same time, the median PGV (corresponding to 50% fragility) at four damage states are listed in Table 6. Due to a decrease of the longitudinal and transverse reinforcement ratios, the damage probability of piers in the three optimized bridges is expected to be larger than that in the original bridge. Moreover, the colour rings mark the range of fragility curves of other components (all components except the pier) with PGV=0.4 m/s. It can be easily observed that the damage probability of other components reduces after optimizing. The main reason is that the thin elastomeric bearings decrease the displacement of girder. The phenomenon verifies the reasonability of the previous explanations. It should be

noted that the damage probability of bridge system reduces after optimizing because other components play much more important role in the seismic performance compared with piers. Obviously, in the process of the system-level seismic design optimization, the seismic performance of overall bridge rather than the individual components is firstly taken into account. Overall, the design optimization method provides a tool that adjust the damage grades of various components by considering the contribution of various components.

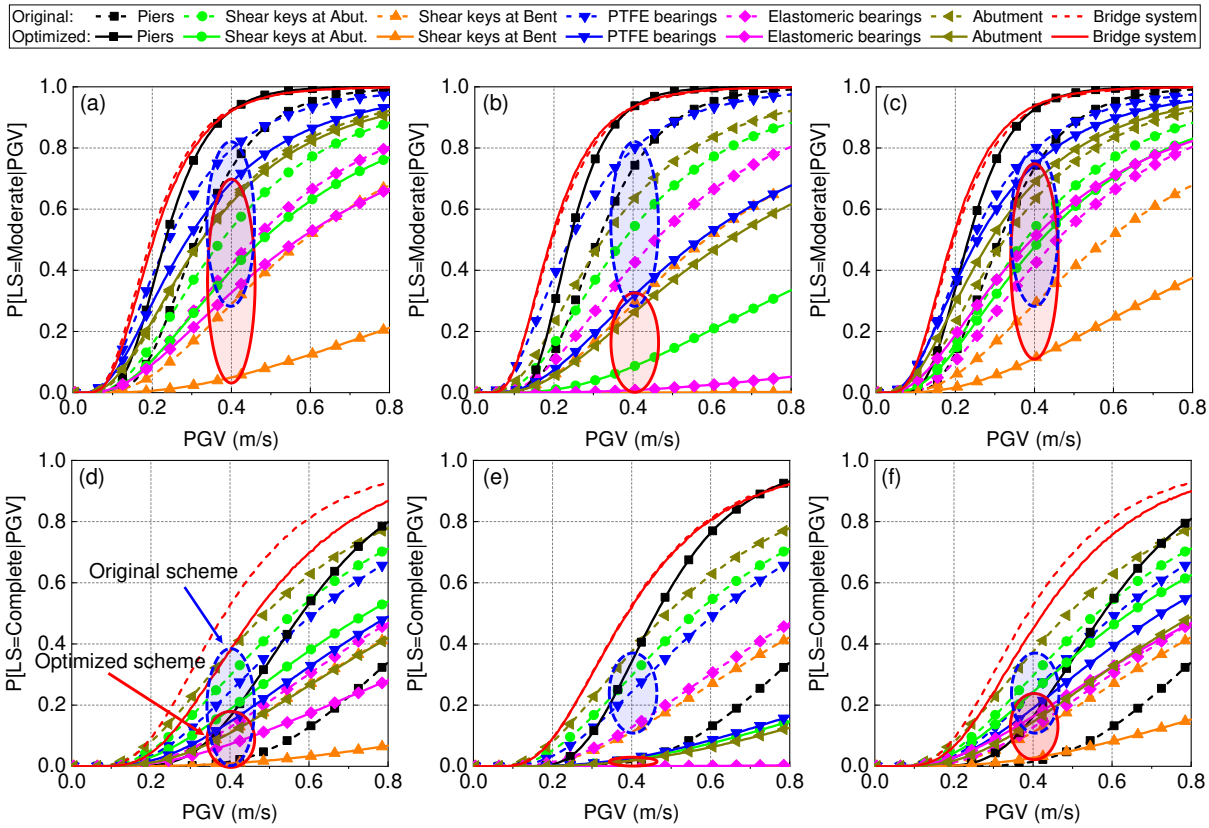

Fig. 14 Fragility curves of components and bridge at four damage states: (a) slight damage, (b) complete damage

Table 6 Median PGV of various components and bridge system with different design schemes

	Original	Opt. 1	Opt. 2	Opt. 3
Slight damage state				
Pier	0.236	0.189	0.210	0.189
Shear keys at Abut.	0.272	0.329	0.750	0.291
Shear keys at Bent	0.403	0.957	-	0.652
PTFE bearing	0.160	0.182	0.358	0.163
Elastomeric bearing	0.282	0.304	1.612	0.214
Abutment	0.315	0.205	0.403	0.184
Bridge system	0.131	0.142	0.159	0.128
Moderate damage state				
Pier	0.313	0.234	0.240	0.233
Shear keys at Abut.	0.377	0.478	1.095	0.417

Shear keys at Bent	0.584	1.542	-	1.024
PTFE bearing	0.241	0.289	0.570	0.257
Elastomeric bearing	0.457	0.570	-	0.393
Abutment	0.324	0.325	0.643	0.289
Bridge system	0.196	0.204	0.193	0.192
Extensive damage state				
Pier	0.605	0.399	0.349	0.397
Shear keys at Abut.	0.422	0.541	1.244	0.469
Shear keys at Bent	0.663	1.806	-	1.186
PTFE bearing	0.406	0.514	1.030	0.458
Elastomeric bearing	0.645	0.890	-	0.602
Abutment	0.370	0.579	1.164	0.516
Bridge system	0.291	0.331	0.286	0.307
Complete damage state				
Pier	0.942	0.582	0.463	0.578
Shear keys at Abut.	0.562	0.747	1.735	0.644
Shear keys at Bent	0.914	-	-	1.764
PTFE bearing	0.613	0.814	1.652	0.724
Elastomeric bearing	0.842	1.264	-	0.850
Abutment	0.490	0.917	1.869	0.816
Bridge system	0.388	0.466	0.391	0.426

Note: "-" means the Median PGV is larger than 2.

In order to verify the computation efficiency of the proposed optimization method, the number of NTHAs for the conventional optimization method and the proposed optimization method are listed in Table 7. It should be noted that the seismic resilience of the conventional method is directly obtained from the seismic resilience analysis. As can be seen in Table 7, the computational cost of the proposed method is much less than that of the conventional method. More importantly, the number of NTHAs is independent of the population sizes for the proposed method. It means that the advantages of the proposed method are highlighted when dealing with the large scale optimization design.

Table 7 Number of NTHAs for different optimization methods (algorithm runs are 40)

Population sizes	50	500	5000
The proposed method	5000	5000	5000
Conventional method	200000	2000000	20000000

Conclusion

This paper presents a seismic optimization method to design the reasonable sizes of elastomeric bearings and the cross-section arrangements of piers in the typical highway RC bridges. The seismic resilience and the material cost of bridge were treated as the optimization functions in the method. The RSM was applied to quickly obtain the seismic resilience and the NSGA-II algorithm was utilized to perform multi-objective optimization. Additionally, the seismic

optimization design was performed on a typical highway RC bridge, and the seismic damage was assessed on the components and bridge system under different design schemes. The main conclusions can be summarized as follows:

(1) The resilience response surface model verifies a good agreement between the predicted values and numerical simulation values. It can be applied to describe the relationship between the design parameters and the seismic resilience of bridges. According to the model, the seismic resilience of bridge system is significantly affected by the diameter of piers, the volumetric ratio of transverse reinforcement, the thickness and area of elastomeric bearings. Whereas, the effect of longitudinal reinforcement ratio on the seismic resilience of bridge system is relatively slight.

(2) The proposed seismic design optimization method realizes minimization of the material cost and maximization of the seismic resilience. The numerical results demonstrate the seismic resilience of bridge system can increase by 8% without increasing the material cost, whereas the material cost can reduce by nearly 30% without decreasing the seismic resilience of bridge system. The efficiency of seismic design optimization can be significant improved by using the resilience response surface model.

(3) The seismic resilience of bridge system depends on the damage grades of various components. The bridge will not always be economic and has better seismic resilience by improving the seismic performance of individual components. The resilience-based seismic design optimization can adjust the damage grades of various components by considering the contribution of various components, entailing an optimal seismic performance and economy of overall bridges.

(4) The Pareto solutions reflect the optimal relationship between the seismic resilience and the material cost. The increase of material cost leads to the seismic resilience increase, whereas the sensitivity of seismic resilience to the material cost decreases. It does not necessarily improve the seismic performance of bridges effectively by the blind increase of material cost. Moreover, the Pareto optimal solutions can be applied to further obtain a simple design formula. The direct resilience-based seismic design can be realized according to the design formula.

Funding

This study was supported by the Natural Science Foundation of Jiangxi Province of China (No. 20192BAB216033) and the China Postdoctoral Science Foundation (No. 2020M671972).

Conflicts of interest

562 No.

563 **Availability of data and material**

564 The datasets used or analysed during the current study are available from the corresponding author on
565 reasonable request.

566 **Code availability**

567 The codes generated or used during the current study are available from the corresponding author on
568 reasonable request.

569 # References

570 Anwar GA, Dong Y, Zhai C (2020) Performance-based probabilistic framework for seismic risk, resilience,
571 and sustainability assessment of reinforced concrete structures. Advances in Structural Engineering,
572 23(7): 1454-1472.
573 Basoz N, Kiremidjian AS (1998) Evaluation of bridge damage data from the Loma Prieta and Northridge,
574 California earthquakes.
575 Billah AM, Alam MS (2015) Seismic fragility assessment of highway bridges: A state-of-the-art review.
576 Struct. Infrastruct. Eng. 11(6): 804-832.
577 Biondini F, Camnasio E, Titi A (2015) Seismic resilience of concrete structures under corrosion. Earthquake
578 Engineering and Structural Dynamics, 44(14): 2445-2466.
579 Bocchini P, Frangopol DM, Ummenhofer T, Zinke T (2014) Resilience and sustainability of civil
580 infrastructure: Toward a unified approach. Journal of Infrastructure Systems, 20(2): 04014004.
581 Box GEP, Wilson KB (1951) On the experimental attainment of optimum conditions. Journal of the royal
582 statistical society: Series b (Methodological), 13(1): 1-38.
583 Bruneau M, Chang SE, Eguchi RT, et al. (2003) A framework to quantitatively assess and enhance the
584 seismic resilience of communities. Earthquake Spectra, 19(4): 733-752.
585 MOHURD (Ministry of Housing and Urban-Rural Development of the People's Republic of China) (2011)
586 Guidelines for seismic design of highway bridges. CJJ 166-2011. (in Chinese)
587 Choi ES, DesRoches R, Nielson B (2004) Seismic fragility of typical bridges in moderate seismic zones.
588 Engineering Structures, 26(2): 187-199.
589 Deb K, Pratap A, Agarwal S, Meyarivan TAMT (2002) A fast and elitist multiobjective genetic algorithm:
590 NSGA-II. IEEE transactions on evolutionary computation, 6(2): 182-197.
591 Dong Y, Frangopol DM, Sabatino S (2015) Optimizing bridge network retrofit planning based on cost-
592 benefit evaluation and multi-attribute utility associated with sustainability. Earthquake Spectra, 31(4):
593 2255-2280.
594 Dong Y, Frangopol DM (2016) Probabilistic time-dependent multihazard life-cycle assessment and
595 resilience of bridges considering climate change. Journal of Performance of Constructed Facilities,
596 30(5): 04016034.
597 Fazli H, Pakbaz A (2018) Performance-based seismic design optimization for multi-column RC bridge piers,
598 considering quasi-isolation. International Journal of Optimization in Civil Engineering, 8(4): 525-545,
599 2018.
600 Fu Z, Gao R, Li Y (2020) Probabilistic Seismic resilience-based cost-benefit analysis for bridge retrofit
601 assessment. Arabian Journal for Science and Engineering, 1-18.
602 Gholizadeh S, Fattahi F (2019) Multi-objective design optimization of steel moment frames considering
603 seismic collapse safety. Engineering with Computers, 1-14.

HAZUS (1999) Earthquake loss estimation methodology, sr2 edn. National Institute of Building Sciences for Federal Emergency Management Agency, Washington (DC).

HPDIMC (Highway Planning and Design Institute of the Ministry of Communications) (2018) Specifications for design of highway reinforced concrete and prestressed concrete bridges and culverts. JTG 3362-2018. (in Chinese)

Hu SC, Wang LH, Li LF, Wu ZH (2019) Time-dependent seismic fragility assessment of offshore bridges subject to non-uniform chloride-induced corrosion. China Civil Engineering Journal, 52(4), 62-71+97. (in Chinese)

Li YJ, Li HN (2018) Interactive evolutionary multi-objective optimization and decision-making on life-cycle seismic design of bridge. Advances in Structural Engineering, 21(15), 2227-2240.

Liu K, Zhai C, Dong Y (2020) Optimal restoration schedules of transportation network considering resilience. Structure and Infrastructure Engineering, 1-14.

McKenna F, Fenves GL, Scott MH (2000) Open system for earthquake engineering simulation. University of California, Berkeley, CA.

Mokarram V, Banan MR (2018) An improved multi-objective optimization approach for performance-based design of structures using nonlinear time-history analyses. Applied Soft Computing, 73: 647-665.

Nielson BG, DesRoches R (2007) Seismic fragility methodology for highway bridges using a component level approach. Earthquake Engineering and Structural Dynamics, 36(6): 823-839.

Pang Y, Wei K, Yuan W (2020) Life-cycle seismic resilience assessment of highway bridges with fiber-reinforced concrete piers in the corrosive environment. Engineering Structures, 222: 111120.

Papavasileiou GS, Charmpis DC (2016) Seismic design optimization of multi-storey steel-concrete composite buildings. Computers and Structures, 170, 49-61.

Papila M, Haftka RT (2000) Response surface approximations: noise, error repair, and modeling errors. AIAA journal, 38(12): 2336-2343.

Rojas HA, Foley C, Pezeshk S (2011) Risk-based seismic design for optimal structural and nonstructural system performance. Earthquake Spectra, 27(3): 857-880.

Shome N, Cornell CA, Bazzurro P, Carballo JE (1998) Earthquakes, records, and nonlinear responses. Earthquake Spectra, 14(3): 469-500.

Sung YC, Su CK (2010) Fuzzy genetic optimization on performance-based seismic design of reinforced concrete bridge piers with single-column type. Optimization and Engineering, 11(3), 471-496.

Verma R, Priestley MN (1990) Optimization of seismic design of single column circular reinforced concrete bridge piers. University of California, San Diego.

Wang Z, Lee GC (2009) A comparative study of bridge damage due to the Wenchuan, Northridge, Loma Prieta and San Fernando earthquakes. Earthquake Engineering and Engineering Vibration, 8(2), 251-261.

Wilson P, Elgamal A (2010) Large-scale passive earth pressure load-displacement tests and numerical simulation. Journal of geotechnical and geoenvironmental engineering, 136(12): 1634-1643.

Xie Y, Zhang J (2018) Design and optimization of seismic isolation and damping devices for highway bridges based on probabilistic repair cost ratio. Journal of Structural Engineering, 2018, 144(8): 04018125.

Figures

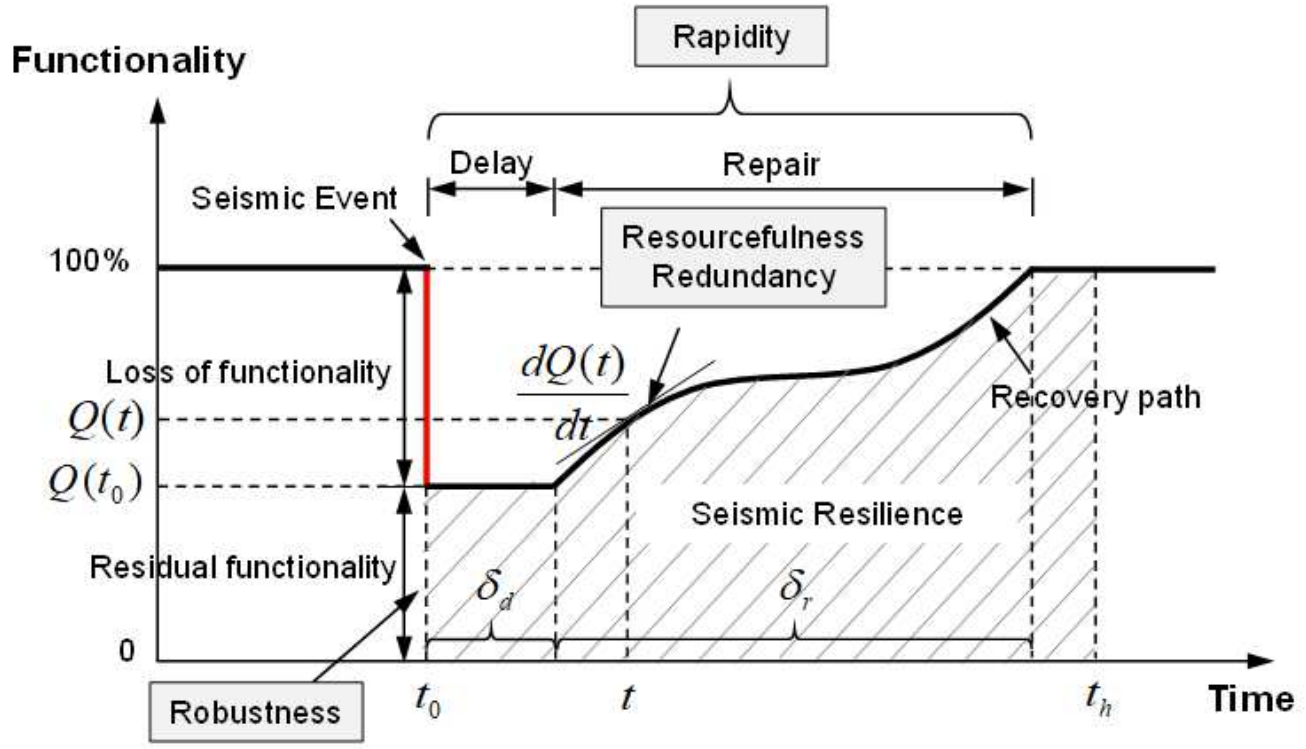

Figure 1

Schematic representation of seismic resilience

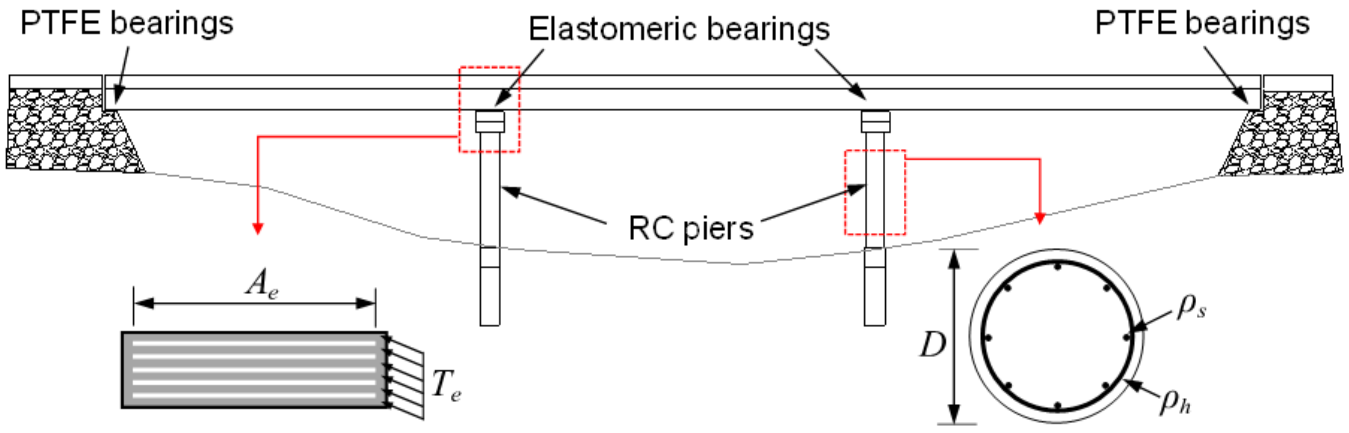

Figure 2

Optimization parameters of the typical RC bridge

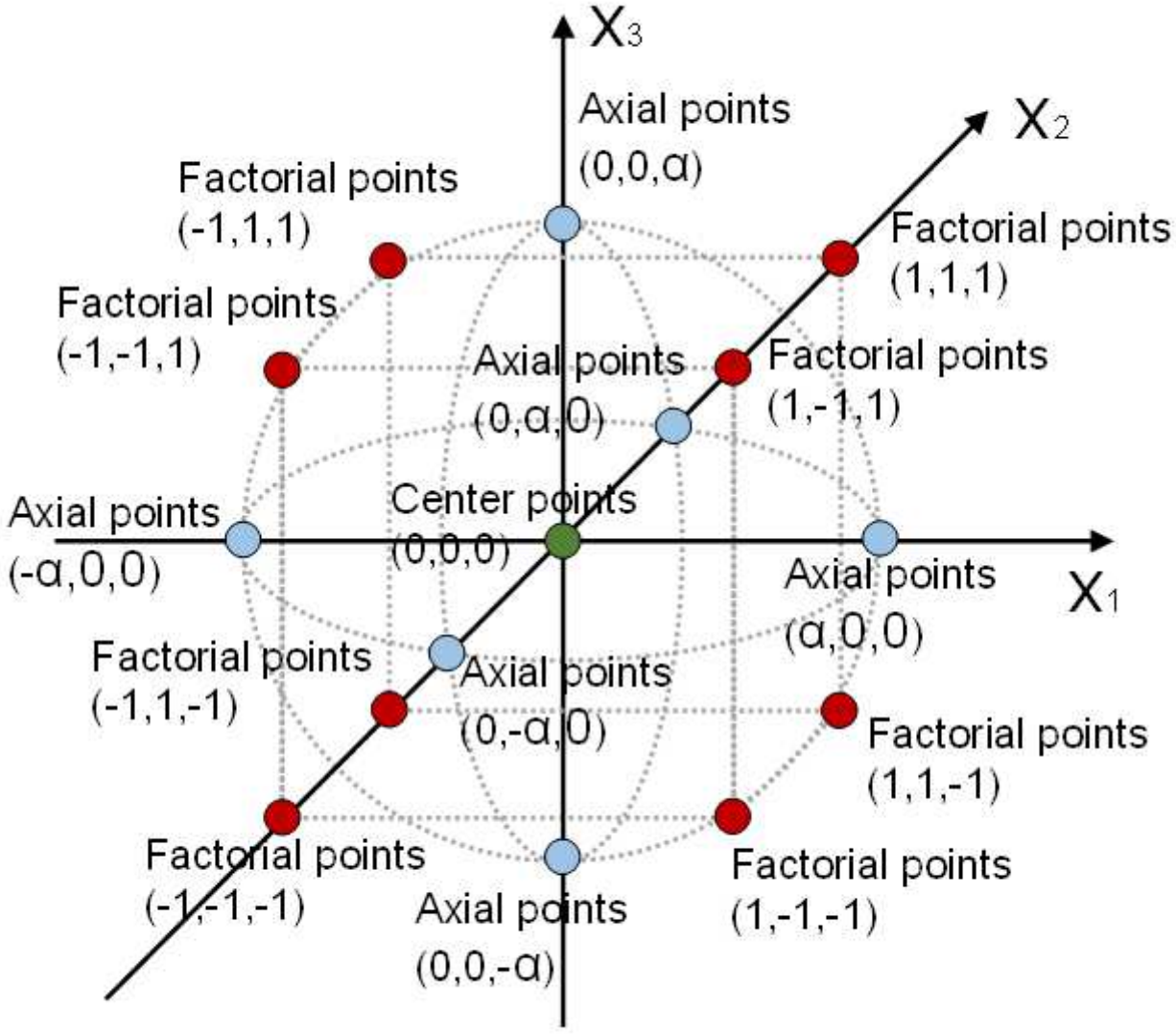

Figure 3

Design points of central composite design method

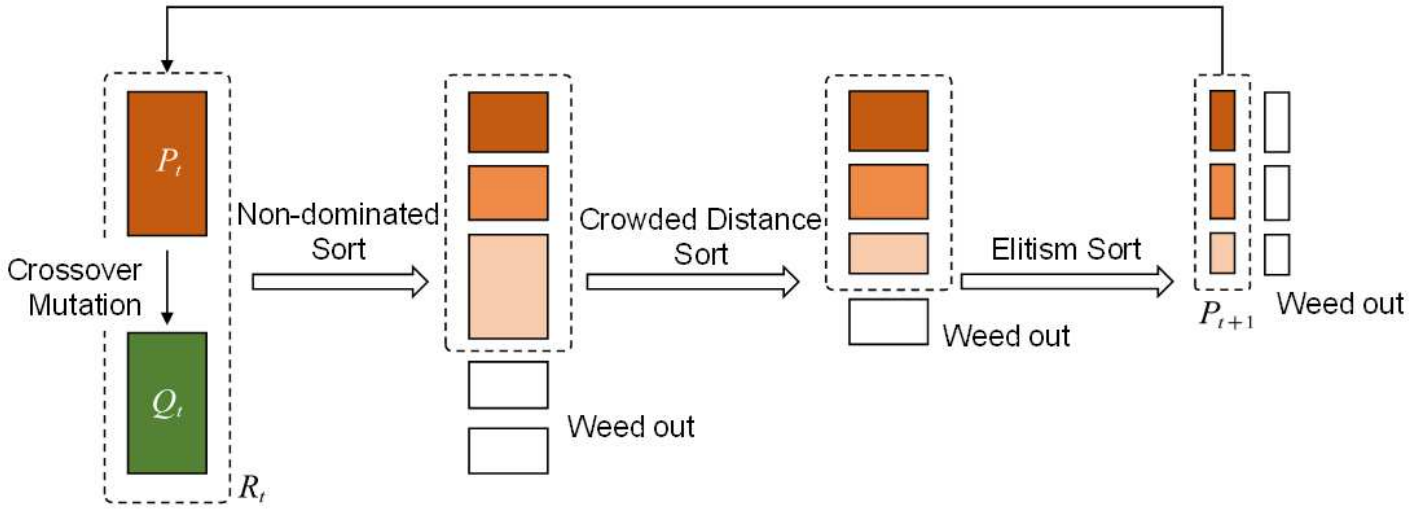

Figure 4

Flowchart of the NSGA-II method

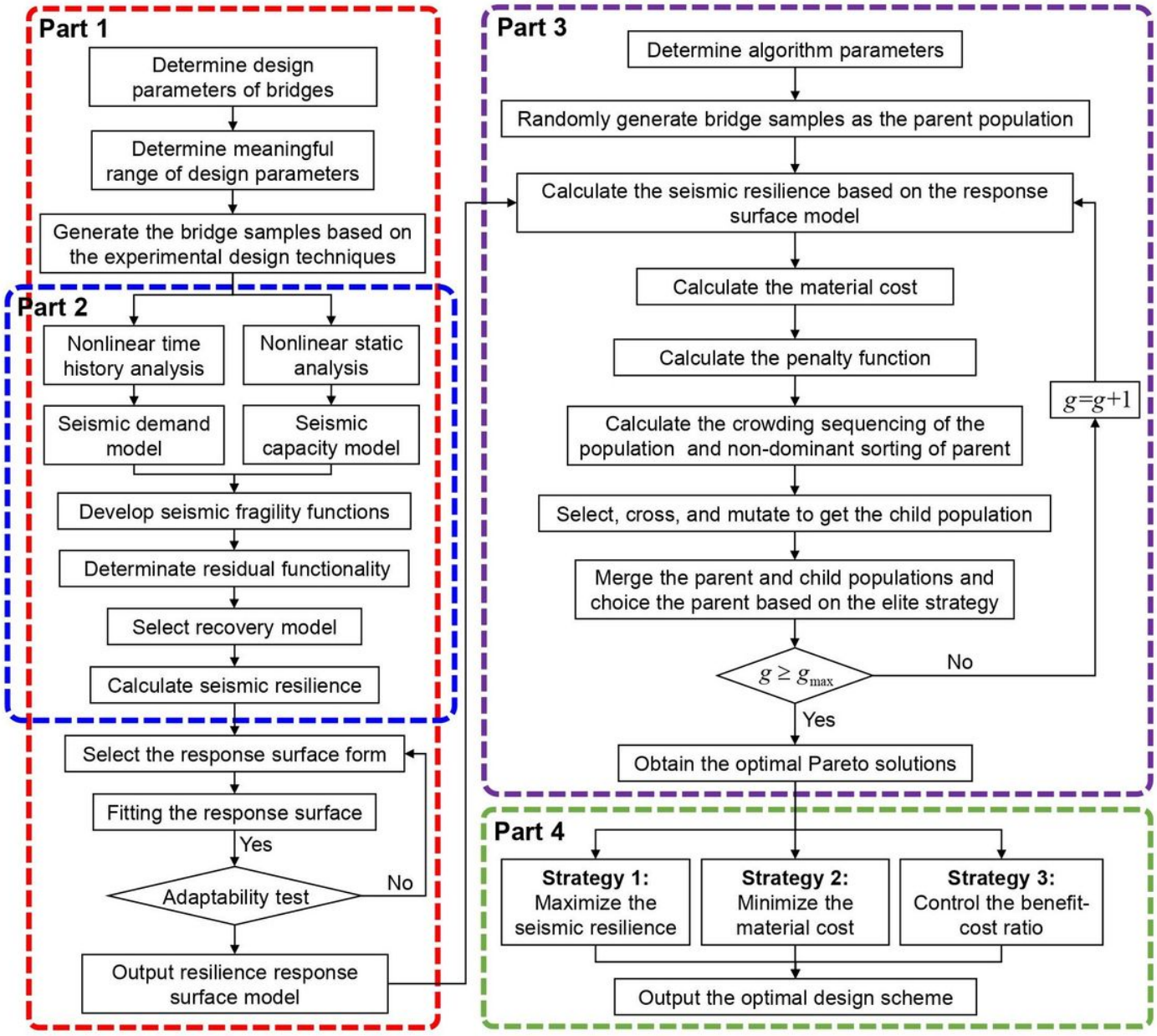

Figure 5

Flow chart of the resilience-based seismic optimization design process of RC bridges using RSM and NSGA-II

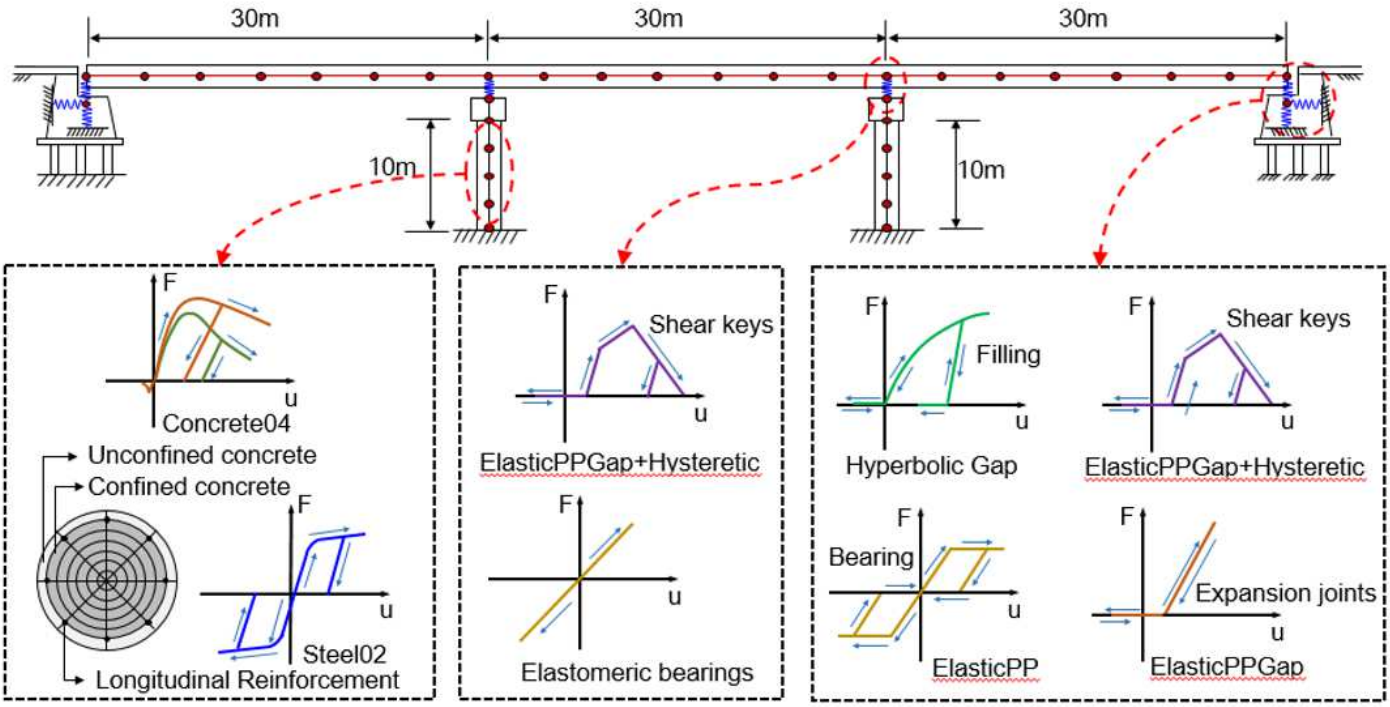

Figure 6

Schematic and finite element model of the case study bridge

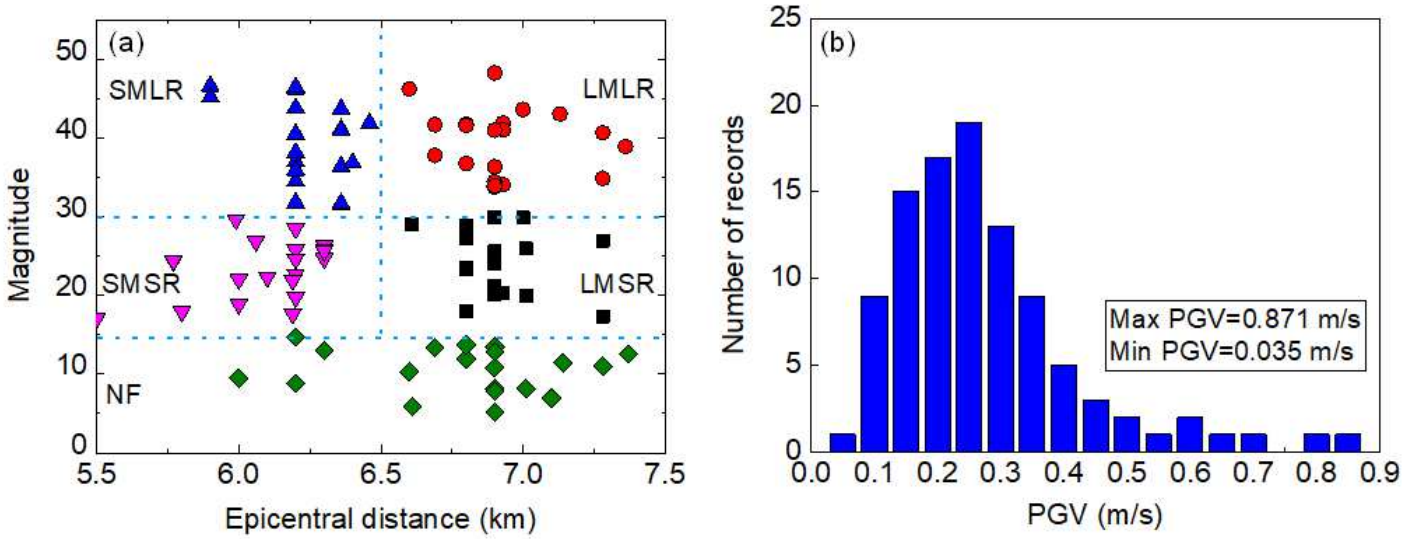

Figure 7

(a) Distribution of ground motion records in M-R space and (b) histogram of the PGV for ground motion records

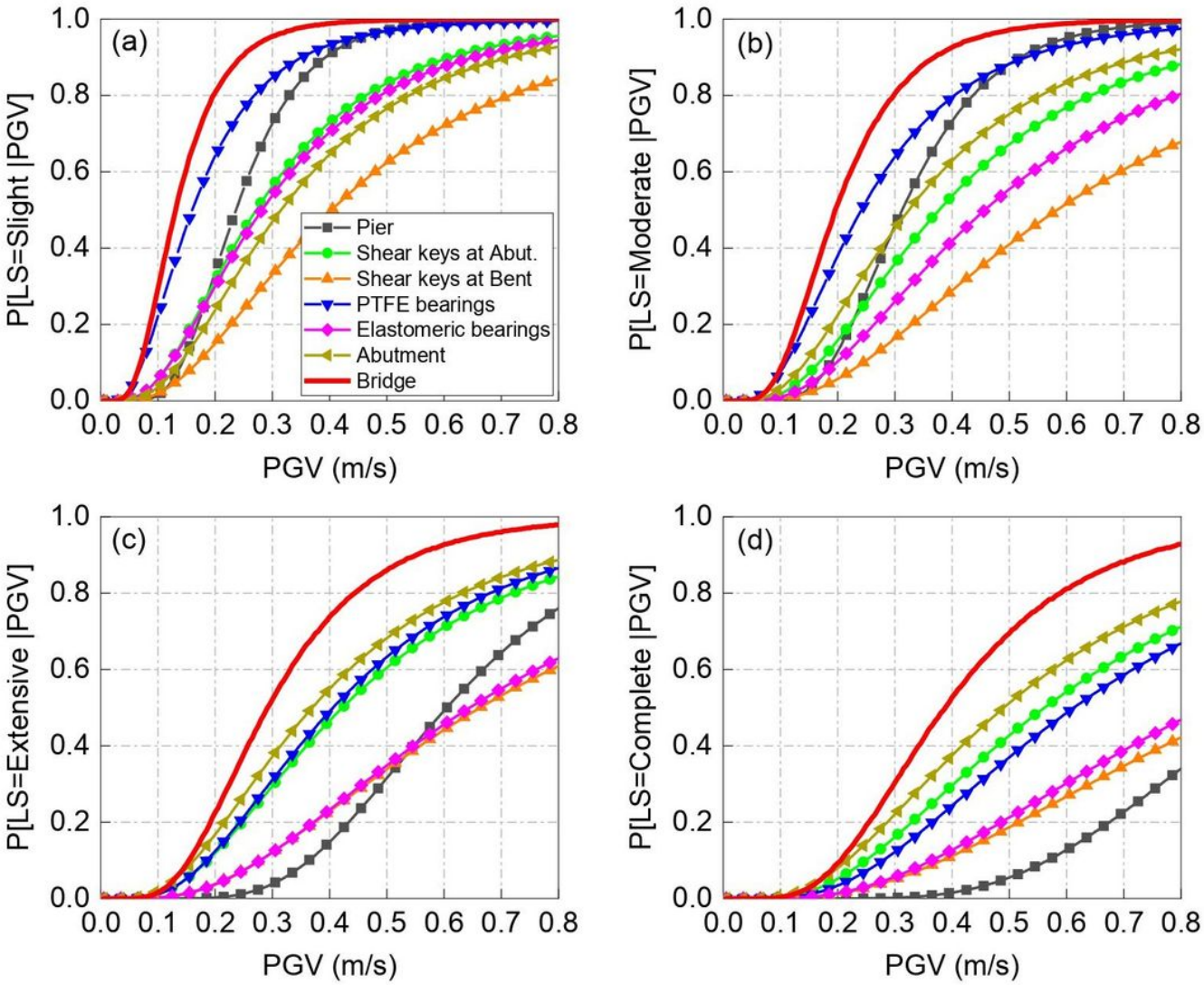

Figure 8

Fragility curves of components and bridge at four damage states: (a) slight damage, (b) moderate damage, (c) extensive damage and (d) complete damage

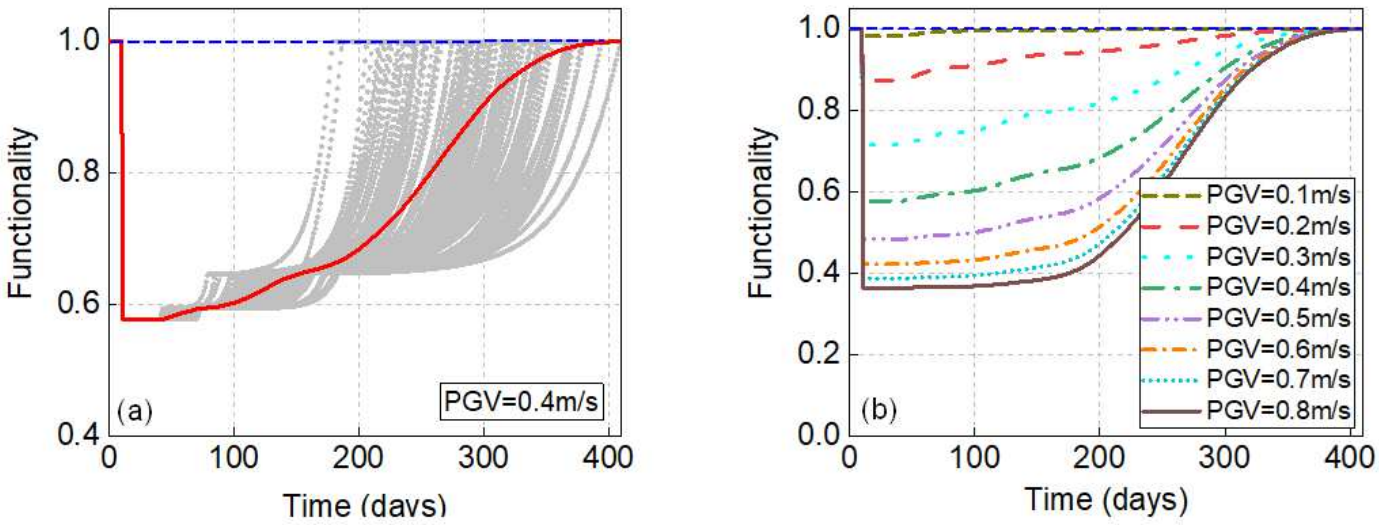

Figure 9

(a) Random samples of functionality recovery processes at PGV=0.4 m/s and (b) average functionality recovery processes with varied PGVs

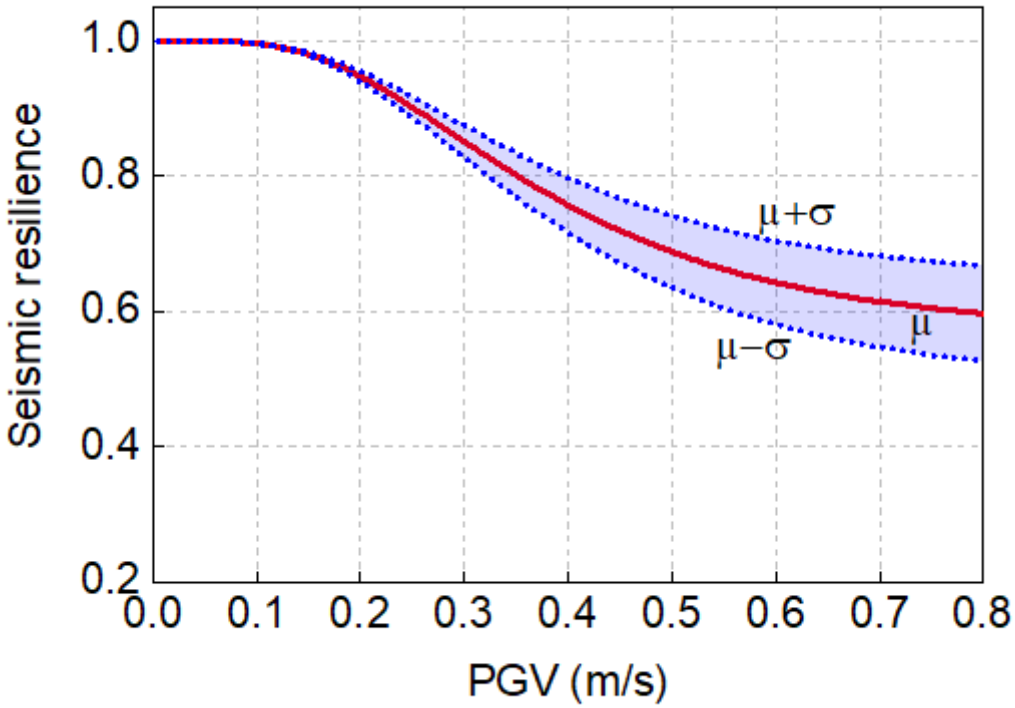

Figure 10

Seismic resilience of bridge with varied PGVs.

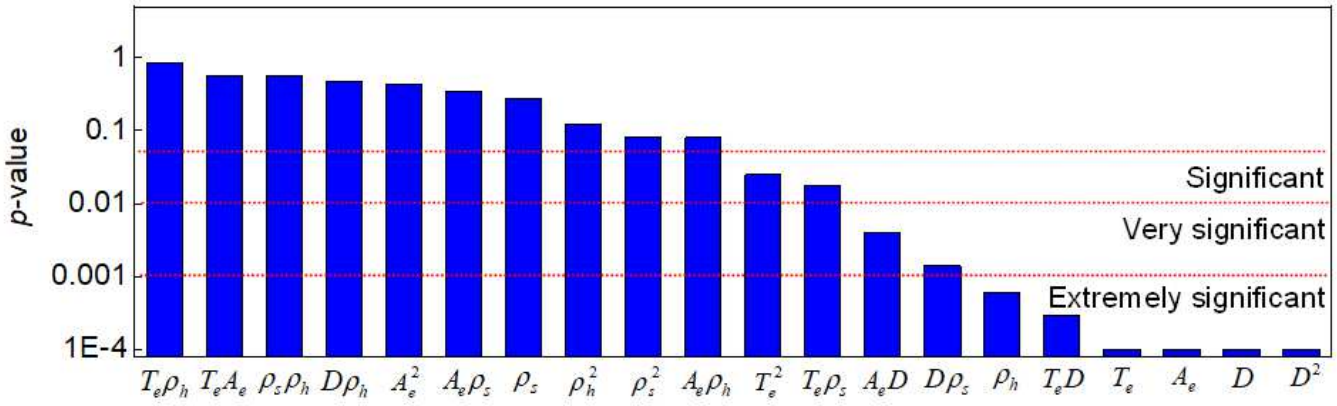

Figure 11

Pareto effect diagram for each factor term.

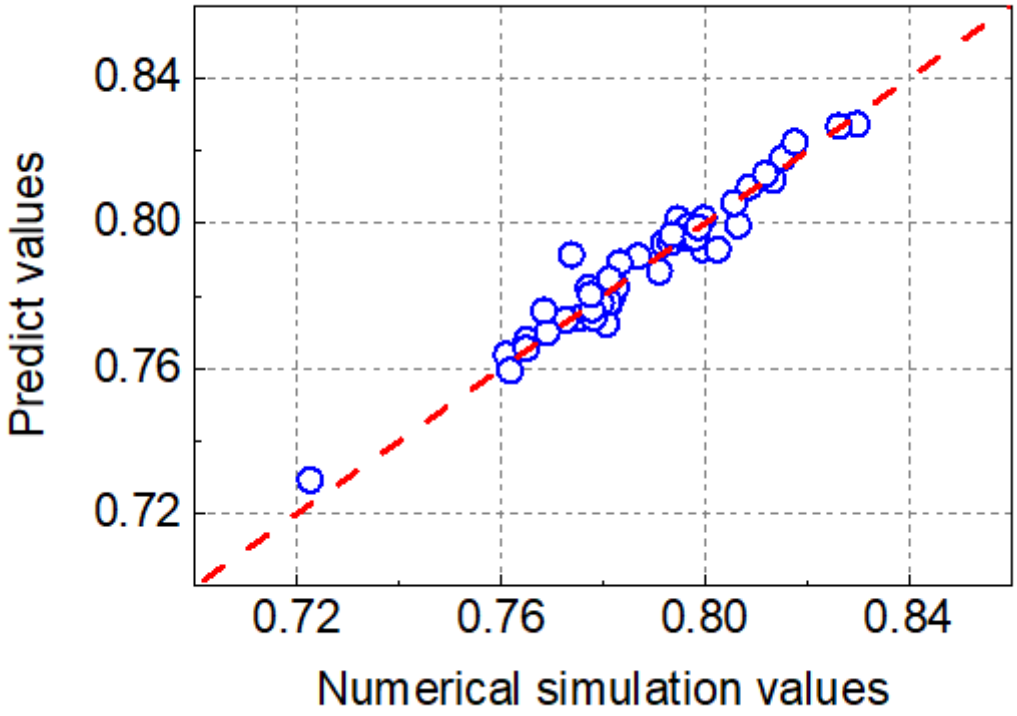

Figure 12

Response variables obtained from the numerical simulations and resilience response surface model.

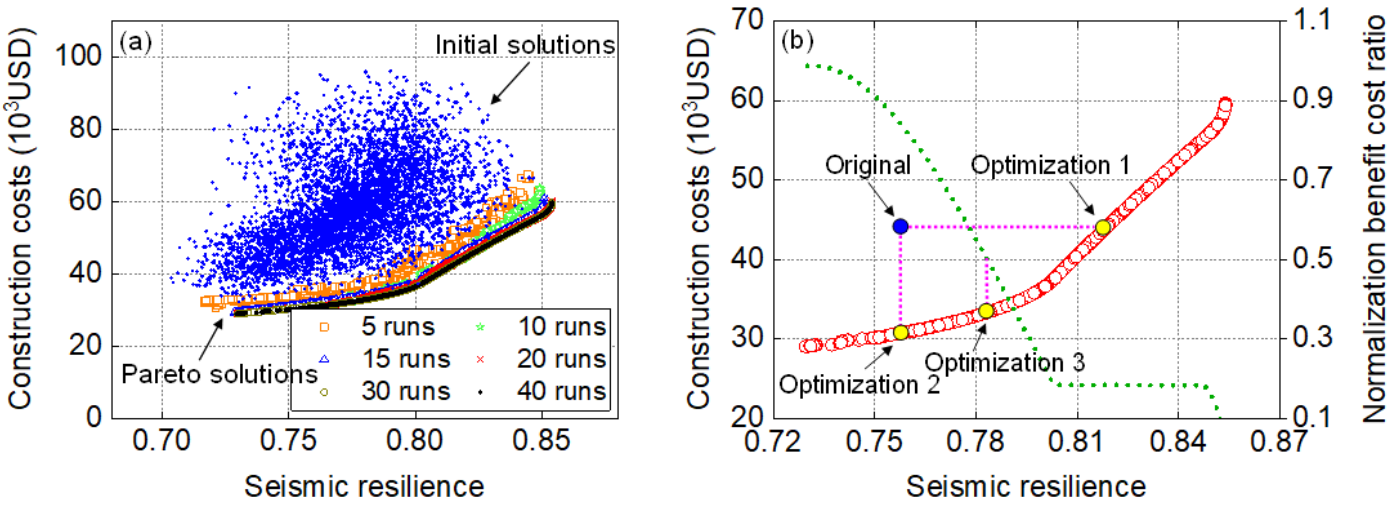

Figure 13

(a) Initial solutions and Pareto solutions with different runs and (b) optimization schemes.

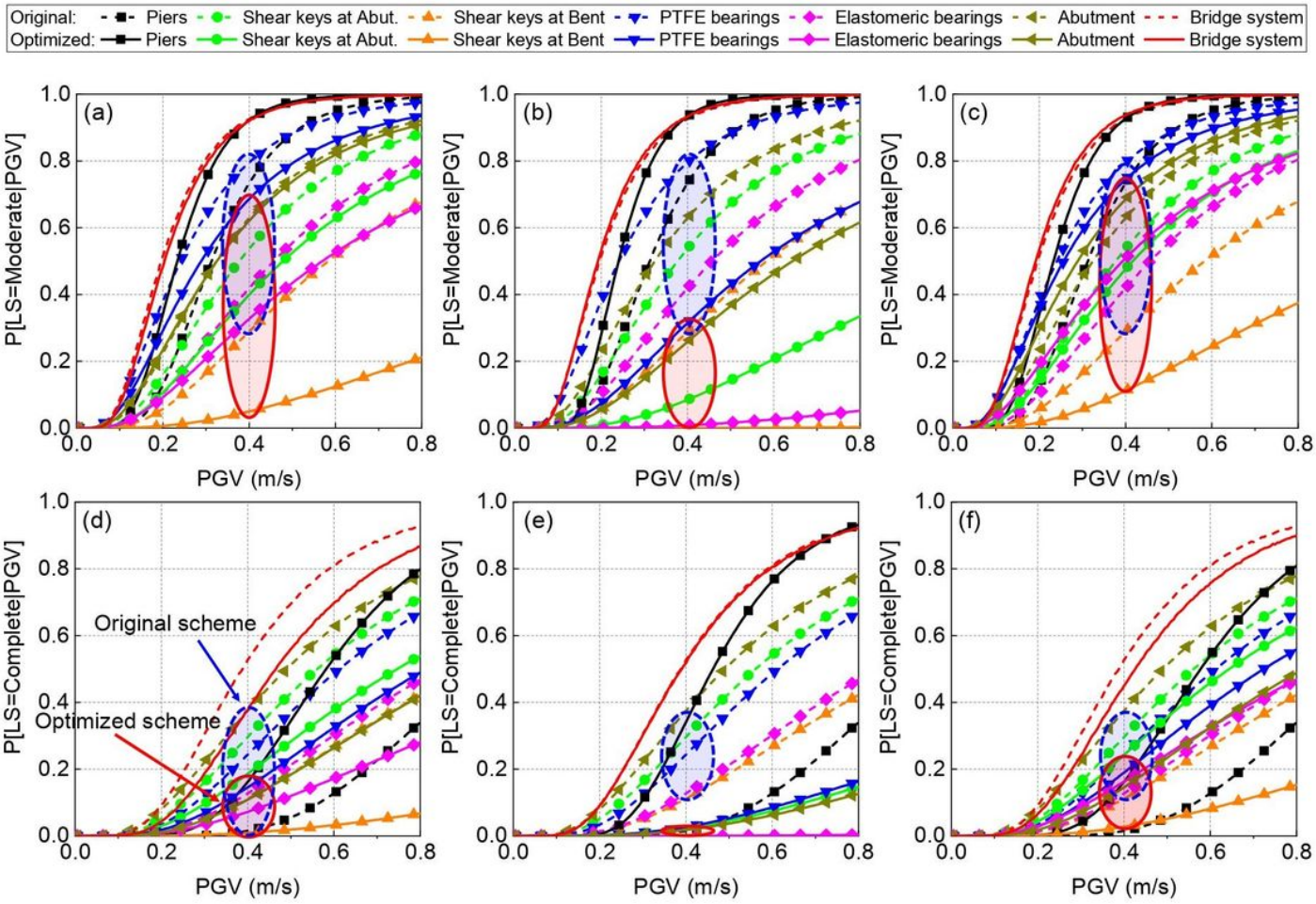

Figure 14

Fragility curves of components and bridge at four damage states: (a) slight damage, (b) complete damage